https://doi.org/10.5194/cp-2023-9
Preprint. Discussion started: 21 April 2023

Climate of the Past Discussions

Southern Hemisphere atmospheric history of carbon monoxide over the late Holocene reconstructed from multiple Antarctic ice archives

Xavier Faïn[1], David M. Etheridge[2,3], Kévin Fourteau[4], Patricia Martinerie[1], Cathy M. Trudinger[2,3], Rachael H. Rhodes[5], Nathan J. Chellman[6], Ray L. Langenfelds[3], Joseph R. McConnell[6], Mark A. J. Curran[13,4], Edward J. Brook[7], Thomas Blunier[8], Grégory Teste[1], Roberto Grilli[1], Anthony Lemoine[1], William T. Sturges[9], Boris Vannière[10,11], Johannes Freitag[12], Jérôme Chappellaz[1,14]

[1]Univ. Grenoble Alpes, CNRS, INRAE, IRD, Grenoble INP, IGE, 38000 Grenoble, France
[2]CSIRO Environment, Aspendale, Victoria, Australia
[3]Australian Antarctic Program Partnership, Institute for Marine and Antarctic Studies, University of Tasmania, Hobart, Tasmania, Australia
[4]Univ. Grenoble Alpes, Université de Toulouse, Météo-France, CNRS, CNRM, Centre d'Études de la Neige, Grenoble, France
[5]Department of Earth Sciences, University of Cambridge, Cambridge, CB2 3EQ, UK
[6]Division of Hydrologic Sciences, Desert Research Institute, Reno, NV 89512, USA
[7]College of Earth, Ocean, and Atmospheric Sciences, Oregon State University, Corvallis, OR 97331, USA
[8]Centre for Ice and Climate, Niels Bohr Institute, University of Copenhagen, Copenhagen, Denmark
[9]Centre for Ocean and Atmospheric Sciences, School of Environmental Sciences, University of East Anglia, Norwich, UK
[10]MSHE, CNRS, Université Bourgogne Franche-Comté, Besançon, France
[11]Chrono-environnement, CNRS, Université Bourgogne Franche-Comté, Besançon, France
[12]Alfred Wegener Institut Helmholtz Zentrum für Polar und Meeresforschung, Bremerhaven, Germany
[13]Australian Antarctic Division, Kingston, Tasmania, Australia
[14]Ecole Polytechnique Fédérale de Lausanne EPFL, CH-1951, Sion, Switzerland

Correspondence to: Xavier Faïn (xavier.fain@univ-grenoble-alpes.fr)

Abstract.
Carbon monoxide (CO) is a naturally occurring atmospheric trace gas, a regulated pollutant and one of the main components determining the oxidative capacity of the atmosphere. Evaluating climate-chemical models under different conditions than today and constraining past CO sources requires a reliable record of atmospheric CO mixing ratios ([CO]) since pre-industrial times. Here, we report the first continuous record of atmospheric [CO] for Southern Hemisphere (SH) high latitudes over the past three millennia. Our continuous record is a composite of three high-resolution Antarctic ice core gas records and firn air measurements from seven Antarctic locations. The ice core gas [CO] records were measured by continuous flow analysis (CFA) using an optical-feedback cavity-enhanced absorption spectrometer (OF-CEAS), achieving excellent external precision (2.8-8.8 ppbv, 2σ), and consistently low blanks (ranging from 4.1±1.2 to 7.4±1.4 ppbv), enabling paleo-atmospheric

https://doi.org/10.5194/cp-2023-9
Preprint. Discussion started: 21 April 2023

Climate of the Past Discussions

interpretations. Six new firn air [CO] Antarctic datasets collected between 1993 and 2016 CE at the DE08-2, DSSW19K, DSSW20K, South Pole, ABN, and Lock-In sites (and one previously published firn CO dataset at Berkner) were used to reconstruct the atmospheric history of CO from ~1897 CE using inverse modeling that incorporates the influence of gas transport in firn. Excellent consistency was observed between the youngest ice core gas [CO] and the [CO] from the base of the firn, and between the recent firn [CO] and atmospheric [CO] measurements at Mawson station (East Antarctica), yielding a consistent and contiguous record of CO across these different archives. Our Antarctic [CO] record is relatively stable from -835 to 1500 CE with mixing ratios within a 30-45 ppbv range (2σ). There is a ~5 ppbv decrease in [CO] to a minimum at around 1700 CE, during the Little Ice Age. CO mixing ratios then increase over time to reach a maximum of ~54 ppbv by ~1985 CE. Most of the industrial period [CO] growth occurred between about 1940 to 1985 CE, after which there was an overall [CO] decrease, as observed at atmospheric monitoring sites around the world and in Greenland firn air. Our Antarctic ice core gas CO observations differ from previously published records in two key aspects. First, our mixing ratios are significantly lower than reported previously, suggesting previous studies underestimated blank contributions. Second, our new CO record does not show a maximum in the late 1800s. The absence of CO peak around the turn of the century argues against there being a peak in Southern Hemisphere biomass burning at this time, which is in agreement with (i) other paleofire proxies such as ethane or acetylene and (ii) conclusions reached by paleofire modeling. The combined ice core and firn air CO history, spanning -835 – 1992 CE, extended to the present day by the Mawson atmospheric record, provides a useful benchmark for future atmospheric chemistry modeling studies.

1 Introduction

CO is a reactive trace gas that plays a crucial role in the interactions between climate and atmospheric chemistry. CO acts on the budgets of both hydroxyl radical (OH) and ozone (O_3), and thus has a strong impact on the global oxidative capacity of the atmosphere. With up to 40% of the OH radicals reacting with CO in the modern troposphere (Lelieveld et al., 2016), CO is the principal sink for tropospheric OH. Consequently, CO indirectly affects the lifetime of many atmospheric constituents such as methane (CH_4), volatile organic compounds (VOCs), and hydrofluorocarbons (HCFCs). Oxidation of CO by OH in the presence of high levels of nitrogen oxides (NOx) can result in significant production of tropospheric ozone, and ultimately leads to CO_2 production (Crutzen, 1973).

CO is produced by atmospheric oxidation of different gaseous precursors and emitted by various surface processes. Atmospheric oxidation of CH_4 and VOCs represents about half of the modern sources (Duncan et al., 2007). Modern terrestrial sources mainly include biomass burning (van der Werf et al., 2017) and incomplete combustion of anthropogenic fossil fuels and biofuels (Hoesly et al., 2018), with minor contributions from the ocean (Conte et al., 2019) and plant leaves (Tarr et al., 1995; Bruhn et al., 2013). Oxidation by OH is the dominant sink of CO, which results in a modern mean global CO tropospheric lifetime of about 2 months (Khalil et al., 1999). However, CO lifetime strongly varies with latitude and season, ranging from

20–40 days in the tropics to up to 3 months in polar areas (Duncan et al., 2007). In the pre-industrial (PI), CO emissions from fossil fuel combustion and oxidation of anthropogenic VOCs were negligible, and limited variations in the methane-oxidation CO source were likely as a consequence of relatively stable atmospheric CH_4 mixing ratios. Thus, the CO budget is expected to be driven principally by biomass burning and oxidation of biogenic VOCs (BVOCs), thereby providing an opportunity to use PI atmospheric CO to reconstruct past biomass burning.

Vegetation fires are an important component of the climate system. Fire emissions affect atmospheric chemistry and composition, biogeochemical cycling, radiative balance, or surface albedo (Archibald et al., 2018, Bowman et al., 2009). Biomass burning is also a major driver of vegetation changes and of ecosystem dynamics (Bond et al., 2005). In return, changes in climate (e.g., variations in temperature or precipitation) drive changes in fire as well as changes in vegetation that provide the fuels for fire. Understanding past fire dynamics is required to improve understanding of the climate-fire relationship on centennial and millennial time scales, which will be essential to project future biomass burning and climate change. There is still a debate about how biomass burning emissions varied in the past and the extent to which humans have impacted the natural fire system (Vannière et al. 2016).

Numerous proxies, exhibiting varying atmospheric lifetimes and consequently different footprints, have been investigated to reconstruct past biomass burning. These proxies, which include southern Hemisphere (SH) reconstructions of Antarctic [CO] (Wang et al., 2010, Haan et al., 1996, 1998), generally suggest that SH biomass burning was high during the medieval period (MP) spanning 1000–1500 CE, with a decrease in burning during the 1400-1500 CE period reaching a minimum sometime during the 1600–1800 CE cool period (Little Ice Age or LIA). However, there are inconsistencies between different records regarding the timing and magnitude of changes during the last three centuries, i.e. the transition from the LIA to the industrial times. The Wang et al. (2010) dataset suggests that, following the LIA minimum, biomass burning emissions increased rapidly during the 1700s and 1800s and peaked during the late 19th century at levels roughly 3 to 4 times the modern ones. By contrast, other fire proxies such as ethane (Nicewonger et al., 2018), acetylene (Nicewonger et al., 2020a), or black carbon (Liu et al., 2021; McConnell et al., 2021) indicate that SH biomass burning remained low throughout the 1800s. Improving our understanding of past burning variability requires more fire paleorecords. Specifically new [CO] records from Antarctic ice archives are needed to document biomass burning history in the SH.

Ground-based and satellite-derived CO data are only available for the last three to four decades. Ancient air preserved in glacial ice and firn is thus a unique archive for reconstructing the past atmospheric CO record prior to the 1990s. Firn is the upper layer of an ice sheet where snow is slowly transformed into ice. A large amount of air can be sampled from the interconnected open pores of the firn. Mean ages of atmospheric gases increase with firn depth. Analysis of air trapped in bubbles in solid ice below the firn layer is required to extend reconstructions further back in time. Over the last decade, Continuous Flow Analyses (CFA) of ice core CO concentrations utilising laser spectroscopy has become a new tool in palaeoclimatology (Faïn et al., 2014; 2022). The CFA-based CO measurements exhibit excellent external precision and achieve consistently low blank levels, with absolute calibration enabling paleo-atmospheric interpretations. Faïn et al. (2022) applied CFA to multiple CO Greenland ice cores, allowing for reconstruction of an atmospheric history for Northern Hemisphere CO over the past 300 yrs.

https://doi.org/10.5194/cp-2023-9
Preprint. Discussion started: 21 April 2023

Climate of the Past Discussions

In this study, we report [CO] firn air depth profiles from seven Antarctic sites, and continuous CO data measured on a set of five Antarctic ice cores. By combining the analysis conducted on these archives, we build a new composite record of atmospheric [CO] in the SH for the last three millennia. This new dataset is compared with [CO] data previously published (Wang et al., 2010, Haan et al., 1996;1998) which suggest an increase of about 100% in biomass burning by the late 1800s, as well as with other biomass burning proxies. We focus on interpreting the pre-industrial trends in atmospheric [CO] largely related to biomass burning and BVOC oxidation sources. Climate-chemistry models and/or Earth System Models can produce simulated atmospheric [CO] at ground level in Antarctica, from the PI era to present-day. Such models are evaluated presently within the Aerosol Chemistry Model Intercomparison Project (AerChemMIP) (Collins et al., 2017). Comparing the past evolution of Antarctic atmospheric [CO] extracted from ice archives for the specific period covering 1850 to present day with AerChemMIP model outputs is out of the scope of this paper. Such comparison, which should also provide improved constraints on inventories of CO emissions, will be addressed in a future study.

2 Sampling and methods

2.1 Firn air samples

Firn air samples used in this study were recovered between 1993 and 2016 from seven different Antarctic sites: Lock-In (LI), Berkner Island (BKN), DE08-2, DSSW20K, DSSW19K, Aurora Basin North (ABN), and South Pole (SP) (Fig. S1). Site descriptions are reported in Table 1. The LI site is located 136 km away from Dome C along the traverse road joining the Concordia and Dumont d'Urville stations (Fourteau et al., 2019). BKN is an island surrounded by the Filchner-Ronne Ice Shelf (Assonov et al., 2007). ABN is located in inland East Antarctica approximately mid-distance between the coast and Dome C, in the Indian Ocean sector. DE08-2, DSSW20K and DSSW19K are located within 20 km of the Law Dome summit, about 120 km southeast of Casey Station (Etheridge et al., 1996; Trudinger et al., 2002).

https://doi.org/10.5194/cp-2023-9
Preprint. Discussion started: 21 April 2023

Firn air sampling site (Fig. S1)	Sampling date	Deepest sampling (m)	Accum. Rate (cm w eq yr^{-1})	Mean annual Temp. (°C)
Lock-In 74°08' S, 126°09' E 3209m elevation	7-14 Jan. 2016	108	3.6 [a]	-53 [a]
Berkner 79°33' S, 45°41' W 900m elevation	10-26 Jan. 2003	63 [b]	13 [b]	-26 [b]
DE08 66°43' S, 113°12' E 1250m elevation	17 Jan. - 28 Feb. 1993	80 [c]	110 [c]	-19 [c]
DSSW20K 66°46' S, 112°21' E 1200m elevation	16-20 Dec. 1997	52	15 [d]	-22 [d]
DSSW19K 66°46' S, 112°22' E 1200m elevation	26-30 Oct. 2004	51	15 [d,h]	-22 [d,h]
ABN 71°10' S, 111°22' E 2690m elevation	25-30 Dec. 2013	102	11.9 [e]	44 [e]
South Pole 90°S, 0°E 2835m elevation	22-23 Jan. 2001	120 [f]	8 [g]	-49 [g]

Table 1. Locations, site characteristics and other relevant information for firn air sampling sites featured in this study. Deepest levels may have experienced contamination during sampling and may not be suitable for paleoatmospheric interpretations. [a] Fourteau et al. (2019), [b] Mulvaney et al. (2002), [c] Etheridge et al. (1996), [d] Trudinger et al. (2002), [e] Servettaz et al. (2020), [f] Butler et al. (2001), [g] Battle et al. (1996), [h] Trudinger et al., (2016).

2.2 Firn air sampling

The firn air extraction technique was originally described by Schwander et al. (1993). Briefly, at each site a shallow ice core drill progressively penetrates the firn column, stopping every few meters to allow recovery of the firn air using a firn air sampling device (FASD). Firn air is sampled at intervals of about 10 m from the surface down to the beginning of the lock-in zone where the age of the gases increases more rapidly. Within the lock-in zone, firn air sampling is typically conducted at intervals of 1-3 m. At each sampled depth, the borehole is sealed by the FASD's inflatable rubber bladder. Two continuous tubes (commonly made of Dekabon, with internal diameter 0.25 in.) pass through the bladder and its end caps. At BKN, LI, ABN, and SP, a "Bender baffle" (e.g., Assonov et al., 2007) was attached below the lower end caps of the bladder for venting firn-air in direct contact with the bladder, while the sample line below the baffle is directed towards gas analysers and canisters (Schwander et al.,1993).

CO sampling from the BKN firn is described by Assonov et al. (2007). The samples collected at the deepest levels of the BKN site were likely contaminated by a leak in the pumping system (Worton et al., 2007) and thus are not included in this study.

https://doi.org/10.5194/cp-2023-9
Preprint. Discussion started: 21 April 2023

Firn air sampling techniques at DE08-2, DSSW19K, DSSW20K and SP are reported by Etheridge et al. (1996), Sturrock et al. (2002) and Rubino et al. (2019). Only two depths (surface and 119 m) at SP were available for our analysis due to a sample pump failure (previous studies have reported full depth profiles for other gases, e.g. Battle et al., 1996).

At LI and ABN, the CO_2, CO, and CH_4 mixing ratios of the extracted firn air were continuously monitored. Specifically, $CO_2$was monitored using an infrared analyzer (LI-COR, LI-7000) and CO and CH_4 with an optical analyzer (SARA, OF-CEAS technology, Morville et al., 2005). These real time measurements were used to indicate when uncontaminated air was extracted from the borehole, and thus samples were only collected when CO_2, CO, and CH_4 contents were stable and below modern ambient levels.

Measurements of ambient air at the DE08-2, DSSW19K, DSSW20K, SP, ABN and LI sites sampled through the FASD were in agreement with measurements of atmospheric air samples collected at Mawson Station and collected at the site (typically 1 ppbv or less discrepancy), suggesting minimal air contamination or loss of CO during firn air sampling. Measurement uncertainty is further discussed in SI Sect. 2.2.

2.3. Firn air CO analysis

The DE08-2, DSSW20K, DSSW19K, SP and ABN firn air samples were analyzed at CSIRO by gas chromatography using a Trace Analytical Reduction Gas Analyser (Langenfelds et al., 2023). Only containers that demonstrated reliable storage for CO were used (glass flasks and electropolished stainless steel tanks) and small time-dependent corrections (e.g. -0.0058 ppbv/day in CSIRO 0.5 L glass flasks fitted with PFA o-rings) were applied to allow for the remaining drift in CO concentration between sample collection and analysis. Uncertainty of CSIRO flask data, including experimental precision and correction for storage, was generally within ±1 ppbv. LI firn air was collected in 3 L stainless steel canisters (Silcocan) pressurized to 3 bars. However, such pressure could not always be reached at the deepest levels sampled, where most of the firn porosity was fully closed. LI samples were measured at IGE (France) in April 2016 (i.e., four months after field collection) using a SARA analyzer (Morville et al., 2005). A subset of LI canisters was reanalyzed 6 months later, demonstrating no [CO] drift related to storage. The BKN firn air was analyzed for CO at MPI using Isotopic Ratio Mass spectrometry (IRMS), along with CO isotopic ratios (Assonov et al., 2007).

Firn air CO analyses conducted at CSIRO are reported on the CSIRO2020 CO calibration scale (see SI for more details). LI firn air CO measurements conducted at IGE are reported on the WMO-X2014 scale. A comparison of CSIRO2020 and WMO-X2014 scales, based on NOAA analysis in 2015/16 of CSIRO's primary standards samples, indicates their consistency within about ±1 ppbv over the 28 - 487 ppbv range (Langenfelds et al., 2023). The BKN CO dataset is reported on the MPI scale, which was 8% higher than the WMO CO_X2004A scale when BKN firn air was analyzed (Assonov et al., 2007). The WMO-X2004 scale gives ~1 ppbv lower values for concentrations below 200 ppbv compared to WMO-X2014 scale, with [CO] reported by Assonov et al. (2007) all below 200 ppbv. Uncertainties reported in this study for BKN firn air [CO] account for calibration scale differences.

https://doi.org/10.5194/cp-2023-9
Preprint. Discussion started: 21 April 2023

2.4. Modeling trace gas transport in firn

Due to diffusional mixing, the composition of firn air at any depth does not correspond exactly to the atmospheric composition at a specific time in the past, rather it is a mix of air over a range of past times so corresponds to a distribution of ages (Schwander et al., 1993). Molecular diffusion through the open porosity of firn, followed by porosity closure, results in increasing gas ages and gas age distribution widths with depth in the firn. Trace-gas records in ice cores are further smoothed by progressive gas enclosure into individual bubbles. Models of gas transport in firn (e.g. Buizert et al., 2012, Witrant et al., 2012, Trudinger et al., 2013) take these effects, and more generally the firn physics, into account and thereby allow reconstruction of past atmospheric variations.

In this study we use the IGE-GIPSA and the CSIRO firn air transport models and inverse models to reconstruct the temporal evolution of CO mixing ratio from our firn depth profiles (Sect. 2.1). The physical basis of the IGE-GIPSA and the CSIRO firn models are described in Witrant et al. (2012) and Trudinger et al. (1997, 2013), respectively. Briefly, these models include molecular diffusion, gravitational settling and advection of air due to firn sinking. Firn models use a site-specific diffusivity-depth profile which is tuned using reference gases that have a well constrained past atmospheric trends (major greenhouse gases and anthropogenic halocarbons). Diffusivity tuning for our seven firn sites has been described in previous studies (Witrant et al., 2012 ; Trudinger et al., 2013, Yeung et al., 2019). The diffusivity-depth profile for DSSW19K was assumed to be the same as for DSSW20K due to their close proximity.

Two different inverse approaches are used to reconstruct atmospheric trends of CO from the firn observations. The IGE-GIPSA inverse model is based on the transfer function approach by Rommelaere et al. (1997) and uses a new definition of the optimal solution (Witrant and Martinerie, 2013) intended to favor robustness (Lukas, 2008). It has already been used to reconstruct several atmospheric trends of trace gas mixing ratios and isotopic ratios (e.g. Helmig et al., 2014, Laube et al. 2016, Trudinger et al., 2016, Yeung et al., 2019 and references therein). The seasonal CO cycle is damped in the firn due to diffusional mixing. The summer minimum is reflected by low near-surface values, and the seasonality variation quickly damps with depth so that below about 30m depth, the CO firn signal mostly reflects annual mean variations (Wang et al., 2012, Petrenko et al., 2013). The IGE-GIPSA inverse firn model cannot reconstruct the CO seasonality (Wang et al., 2012), therefore CO measurements above a depth ranging 30-40 m depending on the site investigated were excluded from the model input. Modeling several firn sites simultaneously to reconstruct a single atmospheric trend provides a much stronger constraint than a single firn site and allows evaluation of the consistency of the firn datasets. Best constraints are obtained when simultaneously modeling firn sites with very different physical characteristics (temperature, snow accumulation rate, etc.) and drilling dates, which is the case for our five sites. The model can use data from firn air pumping and ice core analysis simultaneously, and here we link our reconstruction based on the firn measurements to the end of the ice core record. Trace gas records in ice are affected by an additional smoothing process compared to firn air: bubbles in an ice sample close at a range of times. This process is less well constrained than trace gas transport in firn (e.g. Fourteau et al., 2020) but is driven primarily by the snow accumulation rate which controls the firn sinking speed. Similarly to the approach in Yeung et al. (2019), we use synthetic data points in BKN

https://doi.org/10.5194/cp-2023-9
Preprint. Discussion started: 21 April 2023

Climate of the Past Discussions

ice, which has almost the same accumulation rate as ABN to simulate the constraint from ice core data. The best estimates of CO mixing ratios corresponding to five gas age values ranging between 1882 and 1889 CE were attributed to depth levels with the same gas age in the BKN ice.

The CSIRO inverse model used here is based on the Bayesian synthesis inversion described in Trudinger et al. (2002, 2016) but formulated to infer annual mixing ratios rather than annual sources. As with the IGE-GIPSA inverse model, the CSIRO inverse model infers a single atmospheric trend from multiple firn datasets modeled simultaneously. Both inverse models use Green's functions, which represent gas age distributions, to relate the mixing ratio of a trace gas at the measurement depths to atmospheric mixing ratio of that gas over a range of times (Rommelaere et al., 1997; Trudinger et al., 2002). The modeled CO at a depth in firn can be calculated by convolving the atmospheric CO history with the relevant Green's function (assuming diffusivity versus depth is constant in time). The CSIRO inverse model takes a different approach than the IGE-GIPSA model to the strong influence of seasonality in atmospheric CO on the upper firn mixing ratio profile. Instead of excluding observations in the upper firn, the effect on the firn mixing ratio profile of seasonality in atmospheric CO is calculated with a forward run of the CSIRO firn model forced with a Thoning et al. (1989) fit at daily resolution to the Mawson atmospheric CO record from mid-1992 and mean seasonality calculated from the Mawson record before that. The resulting modeled mixing ratios at the observation depths are subtracted from the firn observations before they are used in the inversion, so that the inversion infers annual values of the atmospheric CO trend up to 1992.0 (with CO from 1993.0 taken from the Mawson atmospheric record). This allows the complete profiles for firn measurements to be used. A melt layer at the DE08-2 site was observed to have been a partial barrier to firn air mixing (Trudinger et al., 1997). The melt layer is advected with the ice downwards away from the snow surface, but this cannot be incorporated into the inversion using the Green's function representation that assumes diffusivity versus depth is constant with time. The influence of the melt layer at DE08-2 is therefore calculated with a forward simulation of the firn model, and the result subtracted from the firn data before the inversion. The CSIRO inversion calculation is regularized by including a term in the cost function to be minimized that is the sum over all years of the change in mixing ratio from one year to the next, as described in Trudinger et al. (2016). At the end of the firn reconstruction, the regularization term compares the final firn reconstruction value with the 1993 to 1997 mean for Mawson. The deep SP firn sample has a small contribution from the atmospheric CO history before 1900 (i.e. part of the Green's function from the firn model for this SP sample extends before 1900). The CSIRO inversion can either reconstruct atmospheric CO from 1900 assuming constant CO before 1900 (the CO value inferred at 1900 is extended back in time and convolved with the part of the Green's function before 1900), or it can reconstruct atmospheric CO from 1898 assuming the atmospheric CO history from the ice reconstruction up to 1897 (the ice reconstruction is convolved with the part of the Green's function extending before 1898), with the regularization described above applied to the change in CO between the last annual ice reconstruction CO value in 1897 and the first annual firn reconstruction value in 1898 (to ensure a smooth and continuous reconstruction from ice and firn). Uncertainties in the CSIRO firn reconstruction are calculated by a bootstrap method (Trudinger et al., 2016) that incorporates uncertainty in the firn measurements, the firn model parameters (using an ensemble of firn Green's functions), the Mawson atmospheric record and the ice reconstruction (when used).

https://doi.org/10.5194/cp-2023-9
Preprint. Discussion started: 21 April 2023

In this study, we apply a multi-site reconstruction inverse method to constrain both the IGE-GIPSA and the CSIRO models and determine the atmospheric reconstruction that fits the investigated sites. Five sites (DE08-2, DSSW20K, SP, LI, BKN) were investigated with the IGE-GIPSA model, and 5 sites (DE08-2, DSSW20K, SP, DSSW19K, ABN) with the CSIRO model. As different models, methodologies and site combinations were used, the comparison of IGE-GIPSA and CSIRO model results provides insights about the robustness of our results.

2.5. Ice core samples

Five ice cores extracted from Antarctica were investigated in this study (Fig. S1). The DC12, ABN, and Taldice (TD) ice cores (Table 2) were used to investigate the past atmospheric history of carbon monoxide over the late Holocene. Two additional Antarctic ice cores, EDML-B40 and Solarice (Fig. S1), which provided complementary and short datasets supporting paleo-atmospheric interpretations, are described in Supplementary information (SI) (Table S3 and SI Sect. 2.6 and 2.7). High resolution CO mixing ratios (See Sect. 2.6) were measured continuously along with those of methane.

Ice core & location	Depth interval (m)	Gas age interval (yrs CE)	Accum. Rate (cm weq yr^{-1})	Mean annual Temp. (°C)
DC12 Dôme Concordia 75°0.6' S, 123°2' E 3233m elevation	108-151; 156-177	1619 ; -835	2.5 [a]	-53 [b]
ABN Aurora Basin 71°10' S, 111°22' E 2690m elevation	108 - 303	1897 ; 22	11.9 (period 1979-2013) [c]	-44 [c]
TD Talos Dome 159°11'E, 72°49' S 2315m elevation	27 sections distributed from 88 to 136 m depth	1876 ; 652	8.6 [d]	-41 [d]

Table 2. Locations, site characteristics and other relevant information for ice cores featured in this study. [a] Gautier et al. (2016), [b] Fabre et al. (2000),[c] Servettaz et al. (2020), [d] Stenni et al. (2002).

DC12 ice core. This shallow ice core was drilled in 2012 at Concordia Station (Dome C) and fully analyzed for CO mixing ratio. The continuous methane record for this shallow Dome C ice core has been reported previously (Fourteau et al., 2020).

ABN ice core. A single summer drilling campaign was conducted in the 2013–2014 season at the ABN site. This drilling site (Servettaz et al., 2022) is located on the lower elevation edge of the East Antarctic Plateau, ~500 km inland of the coastal station Casey, approximately halfway to Concordia station on Dome C (Fig. S1). The entire ABN ice core below close off was analyzed for CO mixing ratio.

https://doi.org/10.5194/cp-2023-9
Preprint. Discussion started: 21 April 2023

TaldIce ice core. The TaldIce drilling was conducted from 2004 to 2008 at Talos Dome, an ice dome on the edge of the East Antarctic plateau and adjacent to the Victoria Land mountain (Stenni et al., 2002; Frezzotti et al., 2007). Talos Dome is located about 290 km from the Southern Ocean and 250 km from the Ross Sea. In the frame of this study, discontinuous sections spanning 19 meters were analyzed.

These three sites experience accumulation rates ranging from 2.5 to 11.9 cm weq yr^{-1} and mean annual surface temperature between -41 and -53°C (Table 2). Ice and gas chronologies for the three ice cores are described in Table S1.

2.6. CO continuous flow analyses

Over the past decade, continuous and high resolution CFA-based CO analyses have greatly improved, including lowering the CO blank and characterizing how CO is preferentially dissolved during CFA process so as to establish absolute calibration (Faïn et al., 2022). The excellent precision of CO analyses has been confirmed, and the designs of CFA setups themselves have been optimized to limit the instrumental smoothing and improve signal resolution. These improvements have been reported in detail by Faïn et al. (2022), which describe CO continuous analyses of five ice cores from Greenland. Here we report here the first application of this method to Antarctic ice cores.

2.6.1. System operation

The ice cores listed in Table 1 were analyzed using a continuous ice core melter system coupled with online gas measurements (Stowasser et al., 2012; Fourteau et al., 2017; Faïn et al., 2022). Ice core sticks are cut at a 34 mm x 34 mm cross section and processed on a melter-head located in a cold room. The melter-head is composed of inner and outer collection areas with the inner area dedicated to sample collection. To prevent contamination, a water overflow from the inner to the outer melter-head areas of >10% is created by lowering the sample pumping speed. The water and gas bubble mixture is continuously pumped via a debubbler into a temperature-controlled gas extraction unit maintained at 30°C. The gas/water volume ratio of the sample is about 10% before the debubbler, and 50% after the debubbler. Water sample without gas bubbles is thus also available at the debubbler for complementary chemical analyses in the liquid phase. The gas is extracted along the sample line after the debubbler by applying a pressure gradient across a gas-permeable membrane, (Transfer-Line degasser, Idex). Then, the gas is dried by a custom-made Nafion (Perma Pure) dryer. Finally, CO (and/or CH_4) mixing ratios are continuously monitored along the gas sample flow by a laser spectrometer.

The Idex degassing membrane operated in this study does not recover dissolved gases from the water phase efficiently. Carbon monoxide (or methane) has higher solubility than N_2 or O_2. Consequently, mixing ratios of CO in the gas phase of the sample flow exhibit lower values than exist initially in the ice bubbles. As melting ice contains ~10% air, a 10:90 mixture of synthetic air with known concentration of CO (and/or CH_4) and degassed deionized (DI) water can be introduced into the system via a 4-port valve located directly after the melter head. The water is sourced from a 2 L reservoir degassed by constantly bubbling

https://doi.org/10.5194/cp-2023-9
Preprint. Discussion started: 21 April 2023

Climate of the Past Discussions

ultra-pure helium through it. The air–water mixture follows the same path through the system as the ice core sample before being analyzed by the laser spectrometer. However, it is not fully identical as it includes more components such as an additional peristaltic pump or extra lines. This pathway for synthetic standard analysis will be designed as the "calibration loop" (CL).

The DC12 and TD ice cores were analyzed at the Institut des Geosciences de l'Environnement (IGE, Grenoble, France) in 2014 during two different analytical campaigns (in June and November, respectively). The ABN core was analyzed at the Desert Research Institute (DRI, Reno NV, USA) in October 2015, immediately after the PLACE (Greenland) core (Faïn et al., 2022) without modification of the CFA setup. Descriptions of the IGE and DRI setups are reported by Faïn et al. (2022).

A unique spectrometer (SARA, developed at Laboratoire Interdisciplinaire de Physique, University Grenoble Alpes, France) operating optical feedback cavity enhanced absorption spectrometry (OF-CEAS, Morville et al., 2005) was used to analyze carbon monoxide (and simultaneously, methane) at both IGE and DRI. Detailed description of this instrument, which was used for CO measurements along Greenland ice cores is reported by Faïn et al. (2022). The OF-CEAS instrument was always carefully calibrated before melting ice cores (SI Sect.1.3).

2.6.2. Precision of continuous CO analyses

We apply the Allan-Werle statistical method (Allan, 1966, Werle 1993) to the calibration loop datasets to evaluate Internal precision and stability of gas-CFA measurements. Observed optimal integration time (i.e., time of lowest Allan-Werle deviation) was determined for each analytical campaign, and is larger than 500 s for DRI, and 1000 s for IGE CFA setups (Fig. S2). Gas data were all averaged over a 10 sec integration time (IT). Such IT allowed full resolution of the variability of the Antarctic CO records. Internal precision, defined as twice the Allan-Werle deviation at chosen integration time, was 0.7 and 1.0 ppbv for the IGE (i.e., DC12 and TD) and DRI (i.e., ABN) analytical campaigns (Table S2).

External precision of the continuous CO measurements (i.e., including all sources of errors or bias) was investigated by melting replicate Greenland ice sticks on different days on a gas-CFA setup, yielding 2.8 ppbv and 8.8 ppbv (2σ) for the IGE and DRI CFA setups, respectively (SI Sect. 1.5).

2.6.3. Absolute calibration and accuracy

CFA–based gas records must be corrected for (i) analytical blank and (ii) under-recovery of gases dissolved in the water stream to obtain absolute values on the WMO-X2014 calibration scale. Evaluation of analytical blanks indicated 4.1 and 7.4 ppbv for the IGE and DRI CFA setups, respectively (SI Sect. 1.6, Table S3).

The calibration loop is an appropriate approach to evaluate the magnitude of CO preferential dissolution (Faïn et al., 2022). We hypothesize that CO and methane dissolution follow the same physical laws: consequently, if a calibration loop is able to

https://doi.org/10.5194/cp-2023-9
Preprint. Discussion started: 21 April 2023

reproduce methane preferential dissolution, it should also reproduce CO losses related to dissolution. In the case of methane, discrete datasets allow for an external validation of this CFA internal calibration. In this study, we extracted calibration factors for CO from calibration loop experiments for each CFA setup (SI).

Overall, CO losses driven by preferential dissolution ranged from 6.0 to 7.4%. Replicate measurements show that the fraction of CO not recovered at the outlet of the CFA system was very stable during analytical campaigns, both at IGE and DRI. Based on repeated calibration loop measurements throughout the campaigns we conservatively estimate the uncertainty of the SC factor to be ±1% (2σ).

2.6.4. Signal Smoothing

Mixing of gases and meltwater during sample transfer from the melt-head to the laser spectrometer induces a CFA experimental smoothing of the signal. The extent of the CFA-based damping was determined for each CFA setup by performing switches between synthetic mixtures of synthetic air standards of different CO concentrations and degassed deionized water. Cut-off wavelengths, defined as the wavelength of a sine signal experiencing a 50% attenuation in amplitude, of 1.6 cm and 9.3 cm were observed for the IGE and DRI CFA setups, respectively (Table S2; see SI Sect. 1.3 in Faïn et al., 2022, for a description of differences and similarities between DRI and IGE CFA setups).

2.6.5. Data processing

Contamination resulting from entry of ambient air into the analytical system as breaks in the core was encountered. The SARA spectrometer simultaneously measures carbon monoxide and methane mixing ratios, and such contaminations were characterized by a sharp increase in methane concentration (ca 1900 ppbv) followed by an exponential decrease. Data were manually screened for ambient air contamination.

3. Results and discussion

In this study, we report new CO records from firn air and ice cores, spatially distributed across the Antarctic ice sheet. In Sect. 3.1, we investigate the spatial variability of CO mixing ratios in the modern Antarctic atmosphere. In Sect. 3.2, we describe our CO firn air and ice core records. In Sect. 3.3, we combine all records to reconstruct the evolution of the past CO burden in the Antarctic atmosphere for the last 3000 years. In Sect. 3.4, we compare this new reconstruction with other paleofire proxies, and Sect. 3.5 discusses new insights on SH past fire history.

https://doi.org/10.5194/cp-2023-9
Preprint. Discussion started: 21 April 2023

Climate of the Past Discussions

3.1. Spatial variability of [CO] in the modern Antarctic atmosphere

Before combining multiple [CO] records from firn air and ice archives collected at sites spatially distributed across East Antarctica (Fig. S1), it is important to assess if atmospheric [CO] exhibits similar levels and trends at these sites. Monitoring of [CO] in the Antarctic atmosphere has been conducted routinely by CSIRO and NOAA. Over recent decades, CSIRO has collected atmospheric [CO] at Casey (Loh et al., 2021a), South Pole (Loh et al., 2021b), and Mawson (Loh et al., 2021c). These three stations are distributed across East Antarctica, with South Pole located on the plateau, and Casey and Mawson both located on the coast (Fig. S1). Over the period spanning 1997-2020 CE, CO mixing ratio at the three CSIRO monitoring sites exhibit almost identical and highly correlated patterns (Fig. S5 and S6) as might be expected given the absence of CO sources across Antarctica. We conclude that [CO] records extracted from firn air and ice core archives at the sites investigated in this study (Fig. S1) can be combined to produce a robust history of atmospheric [CO] in the Antarctic atmosphere.

To further investigate the spatial representativity of an Antarctic record based on firn air and ice cores, we compared the [CO] outputs simulated for the year 2000 in the framework of the ACCMIP exercise (Lamarque et al., 2013) and averaged over three latitudinal bands: 30-90°S, 45-90°S, and 70-90°S. The 70-90°S latitudinal band encompasses the Antarctic ice sheet. Average [CO] over the 45-90°S, and 70-90°S areas are similar, with levels of 51.9 and 51.0 ppbv, respectively. An atmospheric [CO] of 54.1 ppbv is simulated for the 30-90°S latitudinal band, i.e. about 5% higher than [CO] simulated over Antarctica. These modeling results are in agreement with observations: the annual mean [CO] difference in CSIRO measurements between Kennaook/Cape Grim (at 40.7° S in Tasmania; Langenfelds et al., 2023) and Mawson and Casey Stations since 2000 CE is only 2.2 ppbv, the coastal Antarctic Stations being lower. These results suggest that the absolute CO concentrations derived from our datasets not only are representative of Antarctica, but more widely of the mid-high latitude Southern Hemisphere (45-90°S) atmosphere. Also, the temporal changes depicted by our composite record probably have a larger spatial significance, including at least the 30-90°S latitudinal band.

3.2. [CO] datasets

3.2.1 Firn air datasets

CO mixing ratio measured in the firn air at LI, BKN, DE08-2, DSSW19K, DSSW20K, ABN and SP are presented as a function of depth below snow surface in Fig. 1a and 1b. The number of depths sampled varies among sites, with firn air collected at 15 depths at LI, and only one deep sample measured for [CO] at SP by CSIRO.

https://doi.org/10.5194/cp-2023-9
Preprint. Discussion started: 21 April 2023

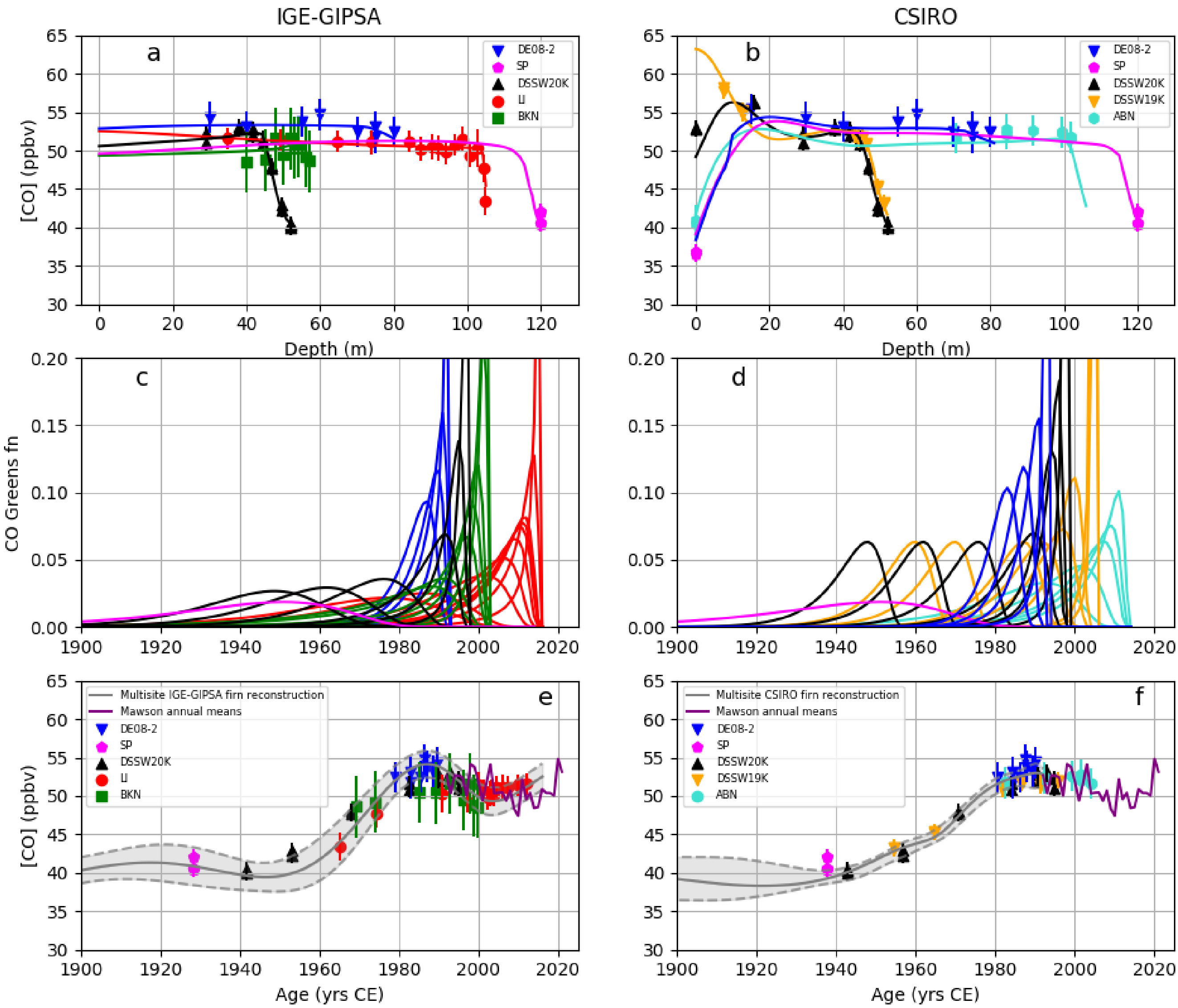

Figure 1. (a) and (b) Depth profiles of carbon monoxide mixing ratio in the firn air at seven Antarctic sites (Lock-In, DE08-2, DSSW20K, DSSW19K, Berkner, South Pole, ABN). Lines show forward model results using optimum atmospheric CO history (Sect. 3.3) as input; symbols are measurements with 2σ uncertainties. (a) reports IGE-GIPSA modeling results: the IGE-GIPSA model does not reconstruct the CO seasonality, and CO measurements above a depth ranging 30-40 m were excluded from the model inputs. (b) shows CSIRO modeling results. (c) and (d) show Green's functions from the IGE-GIPSA (c) and CSIRO (d) firn models (there is one line for each firn sampling depth, with the colors corresponding to those for different sites in panels (a) and (b)). (e) and (f) Best-fit atmospheric history of Antarctic [CO] obtained with the inverse modeling IGE-GIPSA (e) and CSIRO (f) technique (gray line, with the envelope representing 2σ uncertainty). Firn air measurements (symbols) are plotted as a function of mean ages extracted from the modeled age distributions (excluding the upper firn measurements strongly affected by seasonality). We note that firn air data plotted versus mean age are not strictly comparable with the modeled time trends which account for the age distribution widths in the samples. Annual mean [CO] at Mawson Station is shown in purple - the annual means are calculated from a smooth fit at daily resolution to measurements conducted by CSIRO since 1992 on flask samples of background air collected fortnightly (SI Sect. 2.1).

[CO] exhibits a strong seasonal cycle in the Antarctic troposphere, with mixing ratios lower (higher) in summer (in winter) when OH levels are elevated (resp. low) (Fig. S5). The seasonal signal diffuses down in the upper firn layers, and affects the top 30-40 m of the firn depending on the site, with attenuation of seasonality mostly complete below this. Variations in CO mixing ratios observed in the shallowest firn air (Fig.1a and 1b) thus are driven mainly by the atmospheric [CO] seasonal cycle. All firn air sampling described in this study, except DSSW19K, was conducted during summer, and thus surface sampling (denoted as 0 m in Fig. 1a and 1b) exhibited low [CO]. On the contrary, maxima in [CO] are observed at ~10m depth at these sites, reflecting diffusion of elevated wintertime atmospheric [CO] into the firn. Sampling at DSSW19K was conducted in spring (Table 1) and thus exhibits higher [CO] surface levels.

[CO] profiles with depth (Fig. 1a and 1b) differ depending on the sampling site. The oldest and most interesting parts of the firn [CO] records for inferring long-term changes are in deep firn i.e., located below the lock-in depths (Table 1). All sites show a decrease with depth indicating lower atmospheric [CO] levels in the past in the Antarctic atmosphere. Low open porosity of the firn at the bottom of the lock-in zone makes firn air contamination possible during sampling, which results in the partial rejection of measurements at the deepest levels. In this study, we were careful to report only uncontaminated [CO] values. Contamination was identified by deploying specific analyzers in the field ([CO_2], [CH_4] or [CO], sect. 2.2) and/or by detection of anomalous values for species which are expected at very low levels in old air (e.g. halocarbons such as [SF6] or [CFC-11] because they have been emitted to the atmosphere only recently by human activities (Witrant et al., 2012). The [CO] decreases observed in the lock-in zones reveal different shapes. The thickness of the lock-in zone, and the possibility for older gas to be preserved in the firn, depends on climatic conditions such as temperature and snow accumulation (Witrant et al., 2012), which differ between sites. Differences in depth [CO] profiles (Fig. 1a and b) are also related to the age distributions in the firn air samples, which depend on firn physics and on the date of the firn air sampling campaigns (between 1993 and 2016, see Table 1). Interestingly, DE08-2 firn depth profile which was sampled in 1993 (Table 1) exhibits higher [CO] (Fig. 1a). Although some residual contamination or effects of the firn air sampling device can't be ruled out completely in 1993 when firn air sampling was a new methodology, the mean Antarctic atmospheric CO also was higher three decades ago.

Concerns about the potential of CO production on snow surfaces (e.g. Assonov et al., 2007) led us to investigate whether [CO] in firn air and therefore in deeper ice core air could be elevated above background atmospheric levels. Measurements were made of [CO] in air sampled via pump inlets at the snow surface or inserted 5-10 cm into the snow at three regions of Law Dome (a cold, high accumulation region near the summit, a lower accumulation region at DSSW19K and a warmer, snow ablation site near the ice sheet margin). Similar experiment was conducted at Concordia Station (a very low accumulation site where the DC12 ice core was drilled, Table 2), with pump inlets at the snow surface or inserted 10-70 cm into the snow. At all sites, the CO mixing ratios in air sampled during daylight hours at or just below the snow surface were not systematically different, within measurement uncertainty, from those sampled at night or during the day but from about 3 meters above the snow surface. Firn [CO] measurements in the upper 30 m also agree well with the CSIRO model simulations (Fig. 1b) which at this depth range are driven by atmospheric observations at Mawson. From this we conclude that the firn and ice samples are not significantly affected by photochemical [CO] production, presumably due to low CO production in Antarctic snow and/or ventilation of produced CO away from the surface snow layer.

Finally, annual mean values of the CSIRO atmospheric [CO] record from Mawson Station since 1992 CE are also displayed in Fig. 1e and 1f. These direct measurements of atmospheric [CO] in the Antarctic atmosphere, which use the CSIRO2020 calibration scale, exhibit good agreement with firn air datasets.

3.2.2. Continuous [CO] records along Antarctic ice cores

The [CO] new records available from the DC12, ABN, and TD ice cores are reported in Fig. 2 and plotted for a period spanning -835 to 1897 CE (gas age, see Table S1). The high resolution datasets represent the CFA output calibrated (WMO-X2014 scale, Sect. 2.6.3. and SI), vetted for lab air infiltrations (Sect. 2.6.5), with an integration time of 10 s. Splines based on the high resolution signals can be used to produce an average CO history for each site. The envelopes report 2σ uncertainties, and combine uncertainties evaluated specifically for each analytical setup on CO blanks, solubility calibration factors, and external precision of CO CFA measurements (see SI and previous sections). The high resolution DC12 CO record exhibits a 6 m gap, for gas ages spanning -114 to -209 CE, because samples were damaged during transport. To infer the [CO] trend in this missing data interval, we analyzed a section of the Solarice core, which was drilled at Concordia Station in January 2016, 2 km away from the DC12 borehole. Solarice measurements reveal a smooth evolution of CO mixing ratio for the missing period in the DC12 records and we consequently extract a continuous spline from the DC12 dataset (SI Sect. 2.7, Fig. S15). None of the Antarctic records revealed high and variable concentrations that were previously observed in Greenland ice cores and interpreted as in situ CO production (Faïn et al., 2014; 2022). The DC12, ABN, and TD records exhibit stable and low MAD (median absolute deviation) values, with mean MAD values over the entire datasets ranging from 1.1 to 2.4 ppbv, depending on the records. These values are much lower than the MAD values reported for Greenland [CO] records impacted by in situ production, which ranged from 10 to 80 ppbv (Faïn et al., 2022).

https://doi.org/10.5194/cp-2023-9
Preprint. Discussion started: 21 April 2023

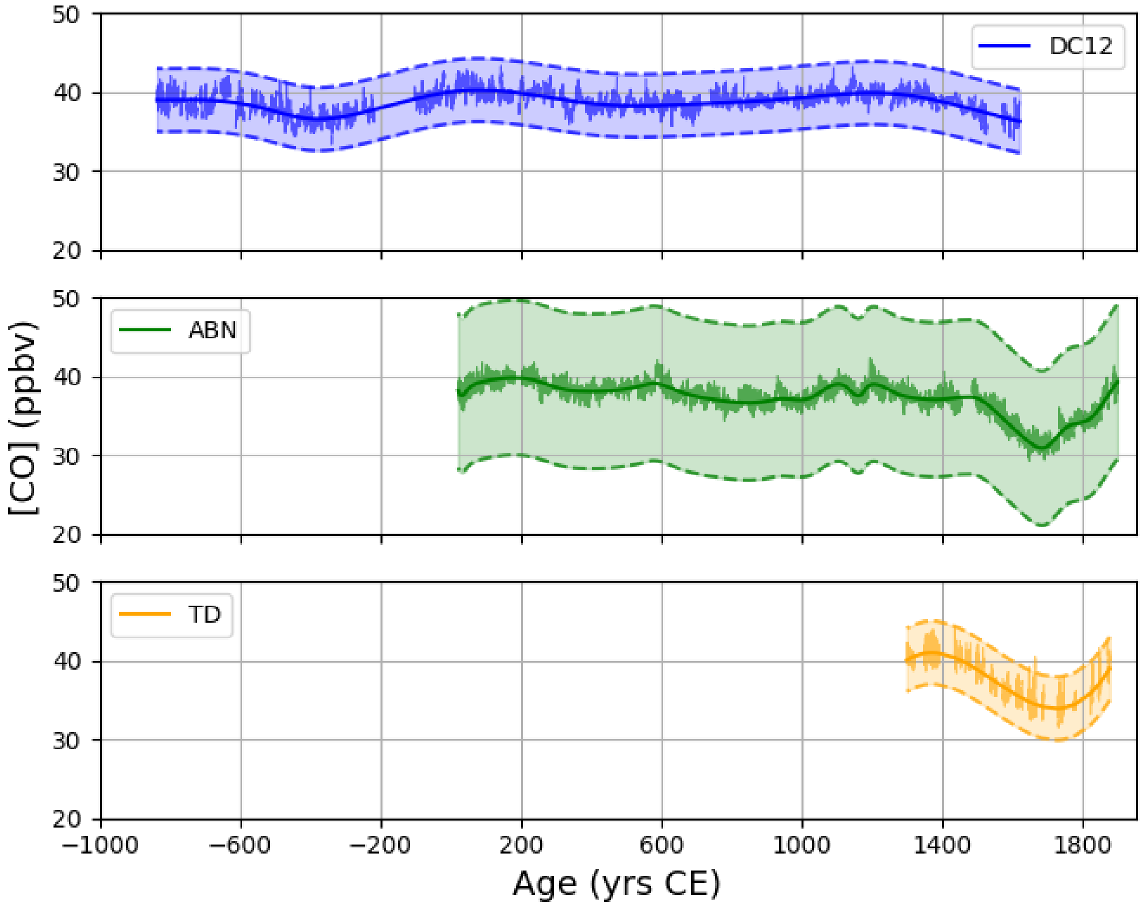

Figure 2. Continuous CO records collected along the DC12 (blue), ABN (green), and TD (orange) Antarctic ice cores. The integration time of high resolution datasets is 10 s. A spline is applied to each high resolution dataset, and the envelopes represent 2σ uncertainties.

The ABN and TD CO records both show a minimum in CO mixing ratio in ~1700 CE. The DC12 record does not extend to 1700 CE, but still shows a decreasing trend in [CO] from 1400 to 1620 CE. All records exhibit rather stable CO levels for periods prior to ~1400 CE. Although some fluctuations in [CO] can be seen prior to 1400 CE, they are not significant compared to the width of the uncertainty envelopes.

The occurrence of a minimum in atmospheric Antarctic [CO] centered in 1700 CE is supported by CFA analyses of the EDML-B40 ice core (SI Sect. 2.6). Although absolute calibration of the EDML-B40 CFA CO dataset was not possible, this record also reveals a minimum in [CO] in the 1700s.

https://doi.org/10.5194/cp-2023-9
Preprint. Discussion started: 21 April 2023

3.3. Atmospheric [CO] history over the last 3000 yrs

3.3.1. A reconstruction spanning 1897 to 1992 CE from firn air data

We applied the inverse IGE-GIPSA and CSIRO firn and inverse models (Sect. 2.4) to reconstruct from [CO] firn depth profiles (Fig. 1a and 1b) the temporal evolutions of [CO] in the Antarctic atmosphere. The IGE-GIPSA reconstruction extends to 2016 CE, and is constrained in 1862-1889 CE by five synthetic data points in BKN ice with mean ages and CO mixing ratios consistent with the ice core composite presented in Sect. 3.3.2. Simulations performed with and without this ice constraint provide consistent results (within uncertainty limits of one another, for more details, see Sect. 2.4 and SI Sect. 2.3.2).

The CSIRO firn reconstruction extends to 1992 CE, after which the atmospheric history follows the atmospheric dataset collected at Mawson station, as described in Sect. 2.4. By using the Mawson record with daily resolution to calculate the influence of seasonality in the upper firn, it is possible to use all of the firn measurements. Fig. S9 shows how the atmospheric history before and after 1992 affects the modeled depth profiles. The CSIRO firn air reconstruction begins in 1898 and uses the ice reconstruction (see Sect. 3.3.2) to give the atmospheric history up to 1897 (with regularization in the inversion preventing the difference between the last ice record value in 1897 and the first firn record value in 1898 being too large). A firn reconstruction run without the ice core record before 1897, instead assuming constant CO before 1900, differs in 1897 from the ice core reconstruction by only 1 ppbv, therefore within the uncertainty envelopes (SI, Fig. S10).

The Green's functions used in the inversions are shown in Fig. 1c and 1d. Optimal atmospheric [CO] histories obtained by both models are reported in Fig. 1e and 1f with the envelope reporting 2σ uncertainty. [CO] firn air data are plotted as a function of mean ages in Fig. 1e and 1f (however note that the Green's functions are a more accurate representation than mean age for the age of firn air, and it is more appropriate to assess the agreement between models and measurements by comparing the CO depth profiles in 1a and 1b than the reconstructed CO time histories and measurements versus mean ages in 1e and 1f). Both IGE-GIPSA and CSIRO firn models were then operated in forward mode to simulate a [CO] depth profile at each firn site from the inferred optimal history (lines in Fig. 1a and 1b). Due to mixing by diffusion, CO mixing ratio profiles in firn are smoothed and the model interprets the CO variability between adjacent depth levels as noise, reflected in the uncertainty envelope. The detailed site by site comparisons of model results with firn data (Fig. S7 and S11), do not show site-specific systematic shifts that would be indicative of inconsistencies between the datasets.

The IGE-GIPSA atmospheric [CO] history based on firn air samples (Fig. 1e) reveals the following patterns: (i) from 1897 to 1945 CE, the record is stable overall with [CO] values remaining in the 37-44 ppbv range; (ii) from 1945 to 1985 CE, the record indicates an increase in [CO] from 37-41 ppbv to 52-56 ppbv, with a mean rate of 0.4 ppbv yr^{-1}; (iii) Antarctic [CO] declines from 1985 to 2000 CE; (iii) over the 2000-2016 CE time period, [CO] slightly increases (+3 ppbv) to reach present-day levels, in agreement with direct [CO] monitoring at Mawson station. The CSIRO atmospheric [CO] record (Fig. 1f)

https://doi.org/10.5194/cp-2023-9
Preprint. Discussion started: 21 April 2023

exhibits a similar pattern, but with the fast increase in [CO] starting ~5 yrs earlier. Overall, IGE-GIPSA and CSIRO reconstructions are in good agreement, always with overlapping uncertainty envelopes.

In this study, we use the two independent models as a way to incorporate firn model uncertainty. Over the period spanning 1920 to 1992, we average the IGE-GIPSA and CSIRO records' annual values to produce a multimodel firn air CO reconstruction. For the 1897-1920 CE period, a polynomial weight was introduced in the annual averaging of the two firn records. Such approach (Fig. S12) allowed (i) to weight the multimodel record toward the CSIRO reconstruction in 1897 CE, and (ii) to match the [CO] growth rates (ie. in ppbv yr^{-1}) of the firn and ice core reconstructions in 1897 and 1920 CE. The multimodel firn air reconstruction is shown in Fig. 3, with the envelope representing the 2σ uncertainty interval.

3.3.2. A reconstruction spanning -835 to 1897 CE from ice core data

Figure 3 reports a history of atmospheric [CO] spanning the last 3000 yr in 45-90°S latitudinal band (Sect. 3.1). Prior to 1897 CE, it is an average multisite record based on ice core continuous datasets. The DC12, ABN, and TD high resolution [CO] records reported along the age scale are merged, and a spline fit of the data from the three sites is used to define the multi-site record. Site specific uncertainties are combined, and the grey envelope reported in Fig. 3 depicts a 2σ uncertainty. The recent atmospheric [CO] history retrieved from firn air (Sect. 3.3.1) covers the period from 1897 to 1992 (Fig. 3).

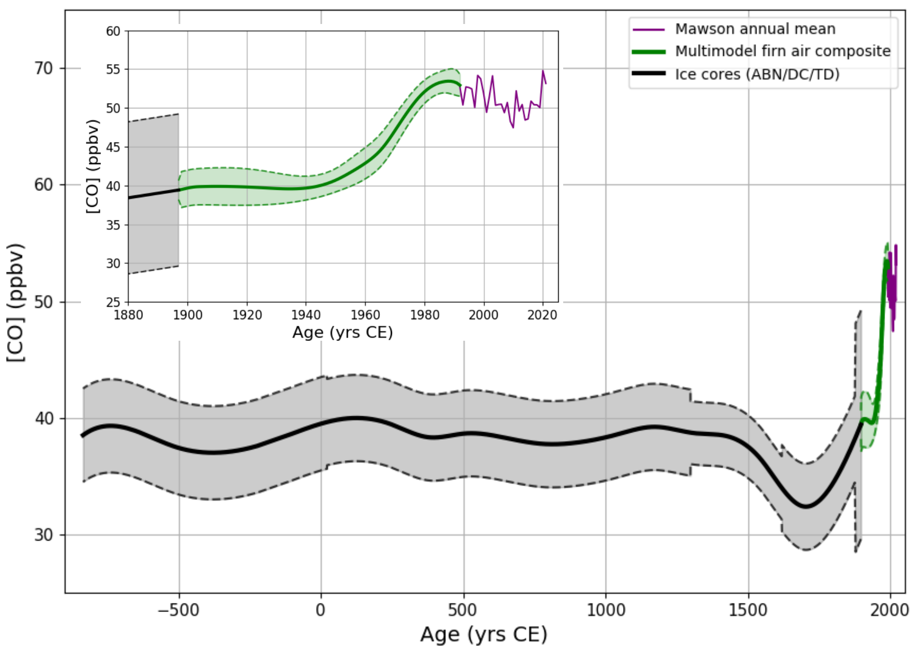

Figure 3. Reconstructed CO mixing ratio in the Antarctic atmosphere for the last 3000 years: a multisite ice core composite (black line) spanning -835 to 1897 CE, and the multisite firn air reconstruction from Fig. 1 (green line) spanning 1897 to 1992 CE. The envelopes represent 2σ uncertainties. Annual mean [CO] at Mawson Station is shown in purple, calculated from a smooth fit at daily resolution to flask sample measurements since 1992. (see text and SI Sect. 2.1). The inset focuses on the last 170 yrs.

https://doi.org/10.5194/cp-2023-9
Preprint. Discussion started: 21 April 2023

Atmospheric [CO] was rather stable from -835 to 1500 CE, with concentrations remaining in a 30-45 ppbv range (2σ). Then, [CO] showed a decreasing trend from 38.5±2.7 ppbv in ~1500 CE to a minimum of 32.5±3.7 ppbv in ~1700 CE. After 1700 CE, [CO] increased until reaching a maximum of 53.6±1.6 ppbv in ~1985 CE. Over the 1700-1900 CE time period, [CO] increased at a moderate rate of 0.035 ppbv yr^{-1}. The subsequent growth rate in SH atmospheric [CO] during the latter half of the 20^{th} century is 10-fold higher (Sect. 3.3.1) than prior to the industrial times (i.e., prior to 1850 CE).

3.4. Comparison with previous ice core CO records

Figure 4 reports a comparison of our new record with [CO] datasets collected earlier from Antarctic ice cores from Vostok (VST, Haan el al., 1998), D47 (Haan et al., 1996; Wang et al., 2010), and South Pole (SP, Wang et al., 2010). Error bars on the VST, D47, and SP represent 2σ uncertainties. The VST [CO] (Haan et al., 1998) which shows stable ~50 ppbv [CO] from -230 to 1370 CE, is only partially shown on Fig. 4. The D47, VST, and SP records suggest stable CO levels prior to 1400 CE, a minimum in [CO] in ~1600 CE, and an increase in [CO] to the onset of the 20^{th} century reaching higher values than today.

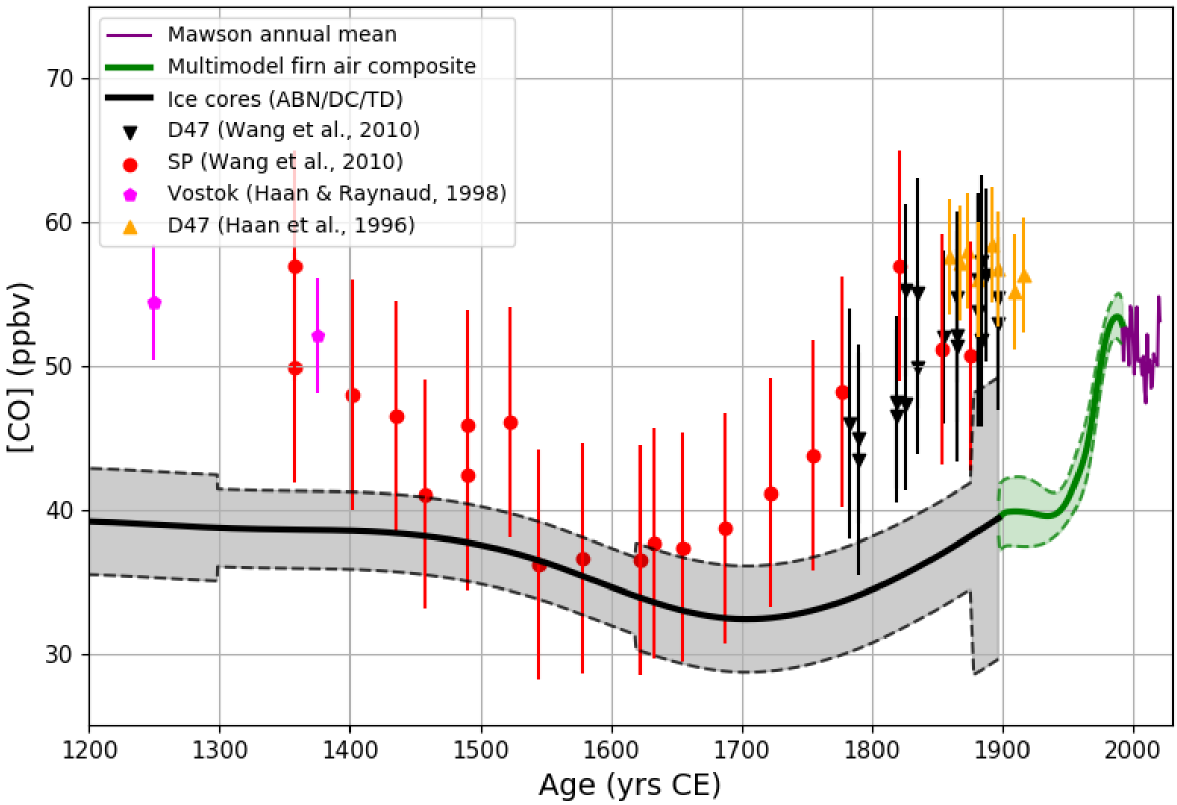

Figure 4. Comparison of the [CO] atmospheric reconstruction based on ABN, DC12, and TD ice core with previously published CO ice core datasets reported with 2σ uncertainties: South Pole (Wang et al., 2010), Vostok (Haan et al., 1998) and D47 (Haan et al., 1996; Wang et al., 2010) archives. Seven more Vostok data points are available in the time period spanning -236 to 1093 yrs CE, with [CO] ranging from 48 to 53 ppbv (Haan et al., 1998).

https://doi.org/10.5194/cp-2023-9
Preprint. Discussion started: 21 April 2023

There are substantial differences between our new record and the published D47/VST/SP dataset. First, the D47/VST/SP dataset exhibits about 10 ppbv higher [CO] than our record prior to 1500 CE, and in the early 1900s (Fig. 4). This difference is larger than our 2σ uncertainty envelope and therefore significant. Such disagreement is puzzling: the published datasets of D47, Vostok, and South Pole agree with each other although they were measured 15 years apart in different laboratories with different analytical methods. On the other hand, our new ice record is internally consistent between the four Antarctic sites (including Solarice core, SI Sect. 2.7). Our new record also includes firn air datasets measured in three different laboratories (IGE, CSIRO, and MPI for the BKN firn air data, Assonov et al., 2007) with different methods, and unlike the earlier records, are contiguous with modern [CO] atmospheric monitoring (Fig. 4). We showed in Section 3.1 that atmospheric CO is relatively uniform over Antarctica, so these differences cannot be explained by spatial gradients between the different ice core sites.

Haan’s studies report [CO] on the CSIRO94 calibration scale which is 3% lower than the CSIRO2020 scale. Wang et al. (2010) calibrated their dataset using a single 141 ppbv gas cylinder certified on the WMO-X2004 scale. The WMO-X2014 scale gives higher values by around 1 ppbv for mixing ratios lower than 200 ppbv compared to WMO-X2004 scale, including for the [CO] range reported by Wang et al. (2010). In this study, consistent calibrations (WMO-X2014 and CSIRO2020) have been applied to all new firn air and ice core datasets. Consequently, a direct comparison of our new record with previously published CO datasets reported in Fig. 4 is possible.

Second, our [CO] record and the South Pole dataset (Wang et al., 2010) both exhibit a minimum during the LIA, but the exact timing of this minimum is different, with our record showing a minimum 100 yrs later than at South Pole (i.e., ~1700 CE, instead of ~1600 CE). The three ice core records in this study all exhibit a minimum in ~1700 CE, i.e. ABN, TD, and EDML-B40 (Fig. 2 and Fig S13).

Third, the amplitude of the decrease in [CO] during the LIA is only 5 ppbv for the new record reported in this study, compared to a 20 ppbv amplitude observed on the South Pole ice core by Wang et al. (2010). We investigated if the ABN and TD records, which constrain in this study a 5 ppbv amplitude for the minimum in [CO] during the LIA, could smooth atmospheric signals by either analytical or gas trapping processes. The response times of the IGE and DRI CFA setup have been documented earlier (Faïn et al., 2022, and SI) and are fully able to resolve the whole amplitude of variation in [CO] observed during the LIA which spans meters (e.g., 40 m along the ABN core). During the LIA, the ABN accumulation rate is lower than modern values (such as reported in Table 1), but it is similar to the South Pole accumulation rate (Servettaz et al., 2022). Thus the ABN record is not expected to be more affected by smoothing than the South Pole record during the LIA. Furthermore, we estimate that the smoothing effect from gas transport in firn and from progressive trapping in ice on the ABN or TD CO ice records is likely insignificant (SI Sect. 2.8, Fig. S16 and S17).

Overall, the lack of consistency between our new record and the published D47/VST/SP dataset is reminiscent of a previous study where we were not able to reconcile the Greenland [CO] Eurocore dataset of Haan and Raynaud (1998) and Haan et al. (1996) with multiple new Greenland ice core CO measurements made using both discrete and continuous analytical methods, including the PLACE ice core drilled 1km away from the Eurocore site (Faïn et al., 2022). Similarly, our Antarctic CO results

https://doi.org/10.5194/cp-2023-9
Preprint. Discussion started: 21 April 2023

call into question the accuracy of the CO values reported for the D47/VST/SP ice core. We could speculate as a possible explanation for the difference that the quantification of CO contamination through the different discrete methods used for the D47/VST/SP ice cores significantly underestimated the true analytical bias introduced by these methods.

An early Law Dome record of [CO] spanning 200-1600 CE was reported by Ferretti et al. (2005). The general pattern of the Law Dome CO record differs from both our study and the D47/VST/SP (Haan et al., 1996, Wang et al., 2010) dataset. Notably, Law Dome [CO] exhibits higher mixing ratios in the 50-90 ppbv range, with no significant decrease in [CO] during the 1400s. The Law Dome [CO] data were a by-product of the methane isotopic measurements by Ferretti et al. (2005) and had significantly higher measurement uncertainty and blank corrections than the dedicated [CO] measurements reported here.

3.5. Implications for pre-industrial SH fire history

In this study, we report an atmospheric history for [CO] in the SH for the last three millennia (Fig. 3). Temporal variations in atmospheric [CO] could, in theory, result from changing emissions of CO and/or changing oxidation of CO during its transport from source areas to Antarctica. Oxidation by OH is the dominant sink of CO but past levels and variations of OH are notoriously difficult to quantify. Based on their ice core isotopic CO dataset ($\delta^{13}C$ of CO), Wang et al. (2010) argued that the PI [CO] variability they observed (Fig. 4) was driven by changes in emissions rather than OH. Earth system models including atmospheric chemistry schemes suggest a stable global average OH-budget from pre-industrial times to 1980 CE (Stevenson et al., 2020). Given the absence of data-based constraints on the OH budget over the last three millennia, we adopt these findings and assume that the PI [CO] variability is primarily driven by changes in emissions rather than changes in the OH sink.

This section therefore discusses the evolution of CO sources and implications for fire history for pre-industrial times. It includes discussion of other proxies of PI biomass burning in the Southern Hemisphere (Rubino et al., 2016a). Such proxies include ethane (Nicewonger et al., 2018), acetylene (Nicewonger et al., 2020a), and black carbon (Liu et al., 2021, McConnell et al., 2021) retrieved from ice cores, and charcoal in sediments (Marlon et al., 2016; Power et al., 2008). Acetylene is released from incomplete combustion processes, and it is lost in the atmosphere via reaction with the OH radical, resulting in a global mean lifetime of roughly 2–3 weeks (Burkholder et al., 2015; Xiao et al., 2007). Biomass burning has been reported as the only major source of acetylene to the pre-industrial atmosphere (Nicewonger et al., 2020a). Ethane is emitted in the modern atmosphere by the production and use of oil and natural gas, burning of biofuels and biomass, and natural geologic seeps (Etiope and Ciccioli, 2009; Helmig et al., 2016; Tzompa-Sosa et al., 2017). The major sink of atmospheric ethane is via oxidation with the OH radical resulting in a global mean lifetime of roughly 2 months (Burkholder et al., 2015; Xiao et al., 2008). Charcoal accumulation in lake or peatbog sediments has been shown to reflect biomass burning within tens of kilometers of the sampling site. Composite stratigraphies based on multiple charcoal records from lake sediments and peats have been built to infer biomass burning history (Vannière et al. 2016; Marlon et al., 2016; Power et al., 2008). Far smaller than charcoal fragments, light-absorbing black carbon (BC) aerosols are primarily emitted from fires during the pre-industrial and can be transported from the SH middle to high latitudes to Antarctica where it get deposited to snow surfaces (Bisiaux et al., 2012;

https://doi.org/10.5194/cp-2023-9
Preprint. Discussion started: 21 April 2023

Liu et al., 2021, McConnell et al., 2021). Overall, these proxies exhibit varying atmospheric lifetimes and consequently different footprints. Stable isotopic composition of methane ($\delta^{13}CH_4$) also has been used to reconstruct the pre-industrial methane budget, including variation of its biomass burning source (Beck et al., 2018; Bock et al., 2017; Ferretti et al., 2005; Mischler et al., 2009; Sapart et al., 2012). However, the atmospheric lifetime of methane is several years and $\delta^{13}CH_4$ is rather a global proxy of PI biomass burning.

3.5.1. Evolution of non-fire CO sources during pre-industrial times

The main sources of CO in the pre-industrial atmosphere are biomass burning and atmospheric production through the oxidation of methane and VOCs. The PI methane-oxidation source is almost constant, as a consequence of the relatively small changes in CH_4 atmospheric mixing ratio prior to 1850 (Rubino et al., 2019). Using a chemical-transport model, Wang et al. (2010) evaluated a nearly constant contribution of the methane oxidation source to [CO] at South Pole in the 10-12 ppbv range for the period spanning 1350-1900 CE. Consequently, SH atmospheric oxidation of VOCs, along with biomass burning, drive the pre-industrial evolution in CO mixing ratio observed in the Antarctic record.

VOCs relevant during the PI are mainly biogenic VOCs. Little is known about past evolution of BVOC emissions in the atmosphere. Isoprene and monoterpenes constitute ~65% of the BVOCs emitted by the terrestrial biosphere (e.g., Guenther et al., 2012), and the processes driving isoprene and monoterpene emissions are complex and still not fully understood (Hantson et al., 2017, and reference therein). BVOC emissions are sensitive to climate, CO_2 concentrations, vegetation type and foliage density. BVOCs emissions from forests account for more than 70% of the total VOC emissions in the 1990s (Guenther et al., 1995). Pongratz et al. (2008) suggest that SH forest area had been fairly constant from 1000 to 1800 CE. Similarly, Goldweijdik suggests that the fraction of land impacted by anthropogenic activities increased from 2.6 to 7.3% between 0 and 1700 CE, reflecting a limited pressure of humans on natural ecosystems and forests prior to industrial times. Using two independent modeling approaches, Acosta et al. (2014) simulate the evolution and driving factors of isoprene and monoterpene emissions during the past millennium. These authors simulate limited decreases in isoprene and monoterpene emissions for the period spanning 1000 CE to 1850, with (i) global isoprene emissions decreasing from 779 TgC yr^{-1} during years 1000–1200 CE to 725 TgC yr^{-1} in 1800 CE, and (ii) a slight decrease in monoterpene emissions between the beginning of the millennium and the pre-industrial time (from 83 to 80 TgC yr^{-1} and from 25 to 24 TgC yr^{-1}, according to MEGAN and LPJ-GUESS models, respectively). They find that climate change can have short-term global effects on isoprene emissions, with e.g., a decrease in BVOC emissions during the LIA. A decrease in gross primary production and a larger decrease in ecosystem respiration was also reconstructed during the LIA using a global numerical simulation of atmospheric carbonyl sulfide (COS) concentrations (Rubino et al., 2016b). Considering the limited variation in atmospheric CO_2, forest coverage and natural landscape prior to 1000 CE, it is unlikely that BVOC emissions have experienced significant changes over the last 3000 yrs.

Evaluating the contribution of BVOC-oxidation to the Antarctic [CO] in PI times requires CO isotope datasets (e.g., Wang et al., 2010) or a 3D chemistry transport model constrained with BVOC emission inventories (e.g., Rowlinson et al., 2021; Sect. 3.5.4). Decrease in BVOC emissions over the last millennia (Acosta et al., 2014) should in principle be reflected by a decrease

https://doi.org/10.5194/cp-2023-9
Preprint. Discussion started: 21 April 2023

in the fraction of atmospheric [CO] produced by the BVOC oxidation source, a decrease possibly enhanced during the LIA (Acosta et al., 2014). However, because such a decrease in BVOC emissions is likely limited, we conclude that atmospheric CO in the SH has not experienced large fluctuation driven by the BVOC oxidation source in PI times.

3.5.2. Evolution of the CO fire source prior to the LIA

Our atmospheric history for [CO] in the SH for the last three millennia reported in Fig. 3 exhibit stable mixing ratios prior to 1500 CE, i.e. the onset of the LIA. Although some variations in [CO] exist, they are not significant within the 2σ uncertainty envelope. The VST [CO] dataset (Haan and Raynaud, 1998) also exhibit stable CO mixing ratios for the period spanning from -200 to 1400 CE (Fig. 4 and Sect. 3.4). The ethane, acetylene and black carbon records retrieved from Antarctica's ice cores exhibit a similar stable pattern from 1000 to 1500 CE (McConnell et al., 2021; Nicewonger et al., 2018), suggesting stable biomass burning emissions during this period.

Regional charcoal indexes are available from the Global Paleofire Database (https://database.paleofire.org). In this study, we extract from this database unpublished regional charcoal indexes for two specific areas: the 30-60°S America and the 30-60°S Oceania latitudinal bands (Fig. S18). Here, we do not consider the Africa charcoal dataset, because southern Africa reaches 33 °S and the density and quality of charcoal records in the African latitudinal band 30-33°S is very low. Furthermore, combining the Global Fire Emissions Database (GFED3; Giglio et al., 2010; van der Werf et al., 2010) and the TM5 chemical transport model (Krol et al.,2005), van der Werf et al. (2013) estimated that CO emissions from fires occurring in Australia and South America are about twice as efficient in impacting Antarctic [CO] as Africa. As expected, sources that are relatively close to Antarctica have more impact on the Antarctic atmospheric [CO]. Charcoal indexes from South America and Oceania areas exhibit the same temporal trend prior to the LIA (Fig. 5), suggesting stable biomass burning for the period spanning from -1000 to 1500 CE.

https://doi.org/10.5194/cp-2023-9
Preprint. Discussion started: 21 April 2023

Climate of the Past Discussions

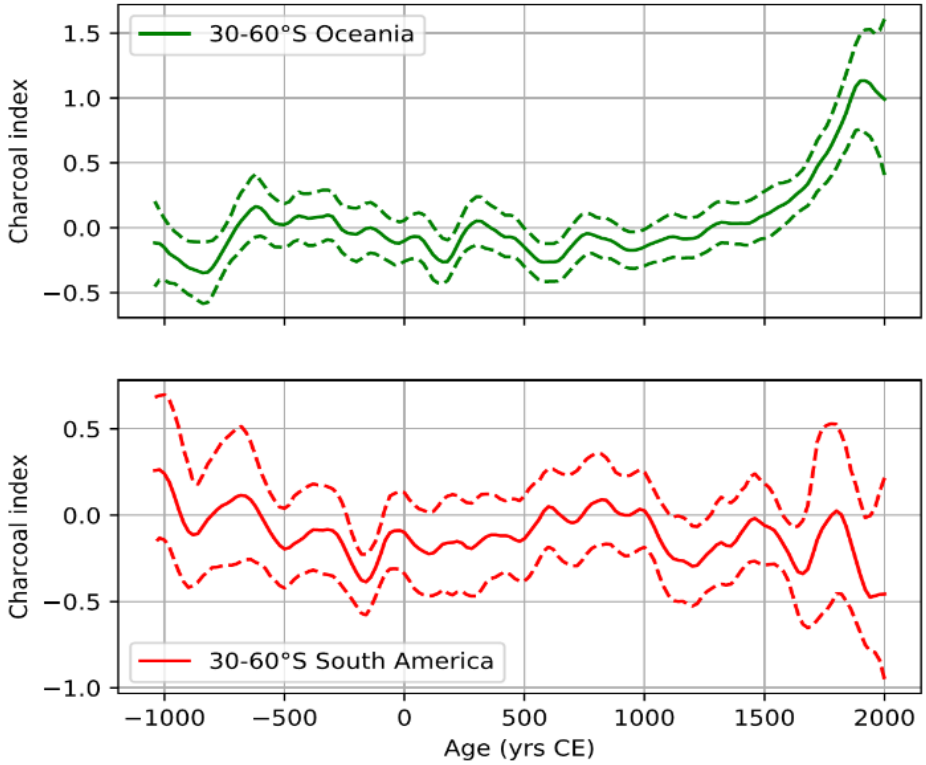

645

Figure 5. Charcoal indexes for the 30-60° S latitudinal band in Oceania (upper panel) and South America (lower panel) for the last 3000 years, extracted from the Global Paleofire Database (https://database.paleofire.org). Charcoal indexes are average Z-scores of transformed charcoal influx per region (100 yr smoothing window/1000 yr bootstrap). Dotted-line envelopes represent the upper and lower 95% confidence intervals from the bootstrap analysis.

Overall, prior to the LIA, charcoal and ice core proxies (black carbon, ethane, acetylene) indicate stable biomass burning levels in the SH. Our atmospheric history of Antarctic [CO] supports this finding - considering the small changes in the methane and BVOC oxidation CO sources (Sect. 3.5.1), stable fire CO emissions are required to explain the stable atmospheric [CO] retrieved from the DC12 and ABN ice cores (Fig. 3).

PI fire modeling conducted by Van der Werf et al. (2013) suggests that the contribution of fire to the Antarctic [CO] in 1400 CE was ~35% below present-day level, with the largest drop due to lower deforestation in South America in 1400 CE. This finding is in disagreement with Wang et al. (2010), who estimated that fire emissions contributed to ~30 ppbv to [CO] in the Antarctic atmosphere in 1350 CE, i.e. a contribution larger than modern fire emissions estimated at 7 ppbv (van der Werf et al., 2013). The lower [CO] levels revealed by our new CO record are thus in better agreement with the paleofire modeling of van der Werf et al. (2013), for the period prior to 1400 CE.

https://doi.org/10.5194/cp-2023-9
Preprint. Discussion started: 21 April 2023

3.5.3. Evolution of the CO fire source during the LIA

Combined continuous CO measurements conducted along the ABN and TD ice cores (supported by the EDML-B40 CO dataset, Sect. SI 2.4) reveal a decrease in [CO] in the Antarctic atmosphere during the LIA, with a minimum around ~1700 CE. Such a decrease is unique over the last three millennia. A slight decrease in BVOC emissions during the LIA (Acosta et al., 2014) may partially explain this decrease in [CO], but a reduction in biomass burning during the LIA is also likely to contribute. Indeed, ethane and acetylene show the LIA as a minimum in burning, with a gradual decline in fire emissions from the MP to the LIA, in the 1500s. This decline is estimated to be 30-45% (resp. 50%) by the ethane (resp. acetylene) datasets (Nicewonger et al., 2018, 2020a). The minimum in the SP [CO] dataset (Wang et al., 2010) was attributed to a decrease in fire emission, using isotopic CO measurements. Charcoal indexes from South America and Oceania areas do not exhibit decreasing trends during the LIA (Fig. 5). However, charcoal signals can be influenced by local and small fires (e.g. caused by human activities) that can mask a regional decrease in biomass burning (e.g., driven by climatic factors). The limited number of charcoal records available also limits the interpretation of charcoal indexes as regional proxies.

3.5.4. Did biomass burning peak at the onset of the industrial period?

The CO records (mixing and isotopic ratios) from Wang et al. (2010) suggest that biomass burning emissions increased rapidly during the 1700s and 1800s and peaked during the late 19th century at rates roughly 3 times modern levels (defined as the 1997–2016 CE period of global satellite records of biomass burning). On the other hand there is no evidence in the three ice core hydrocarbon records (Mishler et al., 2009; Sapart et al., 2012; Nicewonger et al., 2018; 2020a), as well as in the BC Antarctic dataset (Liu et al., 2021), for such a large peak in fire emissions/activity in the late 1800s. The Southern America and Oceania charcoal datasets exhibit opposite patterns at the onset of the industrial period, with increasing fires in Australia, and decreasing biomass burning in Southern America (Fig. 5). Because of such spatial heterogeneities in charcoal indexes, comparing Antarctic [CO] with a hemispheric or global charcoal index (e.g., Marlon et al., 2016) may not be relevant due to lack of documentation, high variability between sites and, finally, poor knowledge of human fire practices, which must include a complex land economy and various land use techniques.

SH biomass burning proxies are used to evaluate biogeochemical and atmospheric chemical transport models that investigate PI biomass burning rates. The output of such models is closely related to PI biomass burning emission inventories. Such inventories are still subject to debate, with contradictory hypotheses discussed. On one side, biomass burning emission inventories (such as the CMIP6 inventories) commonly scale up fire emission with population (e.g., van der Werf, 2013; van Marle et al., 2017), suggesting lower biomass burning emission in PI compared to present day. On the other side, hypothesizing a decline in burned areas with increasing population density due to land use changes (Knorr et al., 2014; Andela et al., 2017) leads to biomass burning reaching higher levels in the PI compared to present day (e.g., Hamilton et al., 2018; Liu et al., 2021, Rowlinson et al., 2021).

https://doi.org/10.5194/cp-2023-9
Preprint. Discussion started: 21 April 2023

Climate of the Past Discussions

Hypothesizing a positive relationship between fire and population density, van der Werf et al. (2013) inferred how PI fire emissions could have contributed to [CO] in the Antarctic atmosphere. These authors find that all the SH non-forest land would have to burn annually or bi-annually to explain the Wang et al. CO levels (i.e., a 30 ppbv contribution from fires to Antarctic [CO] in 1900 CE). They conclude that such a scenario is unlikely, notably because in arid regions, not all savannas build up enough fuel each year to be able to burn annually. Murray et al. (2014) used a chemical transport model (GEOS-Chem) coupled with land cover and fire emissions from dynamic global vegetation models (BIOME4 and LPJ-LMfire) to simulate the PI atmospheric composition. They established a “low PI fire” scenario by scaling the LPJ-LMfire total dry matter consumed to match emissions implied by the charcoal accumulation rates from the Global Charcoal Database (Power et al., 2008, 2010; van der Werf et al., 2010). Such a “low-fire” scenario yields 35 ppbv surface total [CO] at the South Pole in 1770 CE. This value is significantly lower than the SP [CO] of 47±4 ppbv (Wang et al., 2010), but compares well with the 33.5±5.0 ppbv reconstructed in this study (Fig. 3). More recently, Rowlinson et al. (2021) simulated PI [CO] levels using the TOMCAT chemical transport model (which include BVOC chemistry) with CMIP6 fire emission inventory (van der Marle et al., 2017). Simulated Antarctic CO concentration using PI CMIP6 emissions in 1750 CE is 37 ppbv, also substantially lower than the Wang et al. (2010) value of 45±5 ppbv, but similar to our CO reconstruction which exhibits 33.0±5.0 ppbv for CO mixing ratio in the Antarctic atmosphere.

The PI LMfire and PI SIMFIRE-BLAZE fire emissions inventories consider that land use changes imply a decline in burned areas with increasing population density (Hamilton et al., 2018). Similarly, Murray et al. (2014) reported a “high fire” PI fire inventory using the LMFire model and assuming decreases in passive fire suppression (due to less fragmentation in the landscape and reduced live-stock grazing) and the absence of active fire suppression. These three inventories lead to biomass burning reaching higher levels in the PI compared to present days (Hamilton et al., 2018; Liu et al., 2021, Murray et al., 2014), and substantially larger than the PI CMIP6 emissions. Notably, Liu et al. (2021) concluded that fire emissions remained relatively stable in the SH between 1750 CE and ~1920 CE followed by a 30% decrease until about 1990 CE. This conclusion is supported by a comparison of simulated black carbon (BC) deposition fluxes with BC measurement conducted on an array of ice cores (14 Antarctica records, and one record from the Andes). When using SIMFIRE-BLAZE and LMfire emissions, Antarctic [CO] in 1750 CE are estimated at 48 and 61 ppbv, respectively (Rowlinson et al., 2021). The “high fire” inventory reported by Murray et al. (2014) also yields elevated [CO] in the Antarctic atmosphere, with PI concentrations reaching 63 ppbv in 1770 CE. Such values are significantly larger than our continuous CO ice-core record (Fig. 3).

Large uncertainty remains about PI SH biomass burning, with implications for our understanding of the magnitude of the historical radiative forcing due to anthropogenic aerosol emissions (e.g., Hamilton et al., 2018). All fire inventories discussed previously fall within the current uncertainty range for fire emissions (Pan et al., 2020). Although simulating larger PI fire emissions, Hamilton et al. (2018) could not reproduce the enhancement in PI CO emissions from fires reported by Wang et al. (2010), and Liu et al. (2021) do not report a maximum in fire emission in the SH at the onset of the 20th century. The trend and levels of SP/D47 CO SH record (Fig. 3, Wang et al., 2010) are often difficult to reconcile with fire modeling. There again, a possible analytical bias in the estimate of CO contamination by the discrete measurements conducted by Wang et al., 2010,

https://doi.org/10.5194/cp-2023-9
Preprint. Discussion started: 21 April 2023

could explain the discrepancy. Our new SH [CO] atmospheric reconstruction, which does not exhibit a maximum in the late 19th century, is in agreement with paleofire proxies such as acetylene, ethane, methane isotope or BC retrieved from Antarctic ice cores (Nicewonger 2018; 2020a; Sapart 2012, Mischler; Liu et al., 2021), and can bring new constraints on paleofire simulations.

4. Summary and Conclusions

We have produced a firn air record of past atmospheric CO mixing ratio for the high SH latitudes based on 7 different Antarctic firn air sites (Berkner, DE08-2, DSSW20K, DSSW19K, Lock-In, South Pole, and ABN) for the period covering 1897-2016 CE. The quality of this firn air record is supported by the good agreement with direct atmospheric measurements of [CO] at Mawson Station from 1992 CE, which extends the record to 2021. New continuous profiles of [CO] have been measured covering the past 3 millennia by coupling ice core melter systems with online measurements (SARA spectrometer) along four Antarctic ice cores (DC12, ABN, TaldIce, and EDML-B40 archives), with supplementary data from the Solarice core. None of the Antarctic records revealed high and variable concentrations that were previously observed in Greenland ice cores and interpreted as in situ CO production (Faïn et al., 2014; 2022). We calculated a multisite average ice core record, extending the firn air history of [CO] in the Antarctic atmosphere to -835 CE.

Our reconstruction of past atmospheric [CO] at the southern latitudes reveals (i) stable levels prior to 1500 CE at levels of about 40 ppbv, (ii) a ~5 ppbv decrease between the medieval period and the LIA, and (iii) a progressive increase from a minimum of 32.5±3.7 ppbv in ~1700 CE to near present-day levels of 53.6±1.6 ppbv by 1985 CE. This trend relies on an excellent agreement between ten firn air and ice core [CO] records and is contiguous with modern [CO] atmospheric monitoring. Our new CO record exhibits substantial differences with the CO data from the D47, South Pole, and Vostok ice cores (Haan et al., 1996; 1998; Wang et al., 2010): the CO record reported in this study exhibits overall lower levels (e.g., ~10 ppbv lower prior to 1400 CE), a minimum during the LIA occurring about 100 yrs later, and no maximum in [CO] in the late 1800s. Our new [CO] record is in agreement with other ice core SH biomass burning proxies such as ethane or acetylene (e.g., Nicewonger et al., 2018; 2020a) and fire modeling (e.g., van der Werf 2013, Hamilton et al., 2018) that do not reproduce a large biomass burning in the SH at the onset of the 20th century.

Overall, large uncertainties remain on pre-industrial fire history (Nicewonger et al., 2020b), with implication on the PI to modern evolution in aerosol radiative forcing (Hamilton et al., 2018). Nicewonger et al. (2020b) used chemical-transport models to investigate if a single global burning history could be extracted from the three hydrocarbon ice core records. They could not find a consistent fire history even assuming unrealistic changes in spatial distribution of fire and biomes.

These ice-core, firn and atmospheric [CO] measurements, spanning -835-2021 CE, provide a benchmark record of past variations in the high southern latitude [CO] for future atmospheric chemistry model studies. Since the early 20th century,

https://doi.org/10.5194/cp-2023-9
Preprint. Discussion started: 21 April 2023

industrial activities have impacted biogeochemistry resulting in large CO changes (Szopa et al., 2021). Rapid growth in [CO] from the mid 1900s was likely due to combustion sources and the indirect CO production from atmospheric CH_4 oxidation. Disentangling the roles of these sources and possible changes in the OH sink in this [CO] growth and the subsequent [CO] decrease over the past 3 decades involves understanding of the coupled CO-OH-CH_4 system. A natural extension of this work will be the comparison of our ice and firn-based atmospheric [CO] reconstruction for the period covering 1850 to present with model outputs from the AerChemMIP exercise (Collins et al., 2017).

Data availability. The following datasets will be accessible on PANGAEA: (i) ice core high resolution [CO] and multisite ice core [CO] composite, (ii) firn air [CO] and atmospheric [CO] inversions from firn air, atmospheric [CO] from Mawson Station (Antarctica).

Supplement. A supplement related to this article is available

Author contributions. This scientific project was designed by XF, JC, DME, EJB, TB, and MAJC. The high-resolution ice core carbon monoxide measurements were carried out by XF, KF and RHR with support from RG, NJC, and JRM. The firn air [CO] analyses were carried out by RLL, XF, AL and WTS. XF, GT, DME, JC and JF participated in ice core drilling or firn air sampling. The firn air models were developed and implemented by PM and CMT. The codes for data processing were developed by KF, JRM, RLL, PM and XF. Charcoal datasets were processed by BV. All authors contributed to the interpretation of the data. The paper was written by XF with help from all co-authors. Specific methodological sections were written by CMT, PM, and RLL.

Competing interests. The authors declare that they have no conflict of interest

Acknowledgements. We thank the following for firn air sampling: the late J.-M. Barnola (LGGE) at Law Dome in 1993, A. Smith (ANSTO) and the late A. Elcheick (Australian Antarctic Division) at Law Dome in 1998, D. Ferretti (NIWA, New Zealand) at Law Dome in 2004, M. Battle (Bowdoin University), J. Bastide (Bowdoin University), J. Butler (NOAA), and A. Clarke (NOAA) at South Pole in 2001, and D. Spencer and P. Krummel for measurements at CSIRO GASLAB. Grateful thanks go to Olivia Maselli, Larry Layman, Daniel Pasteris, Michael Sigl, and other members of the DRI team who assisted with the measurement campaigns. We thank Sophie Szopa for useful discussions. The French-Italian project SolarIce (IPEV1145, PNRA16_00008) benefited from logistical support from the French and Italian Polar Agencies, IPEV and PNRA, and the F2G for drilling activities at Concordia Station. The French Polar Institute (IPEV) also provided logistical support for

ABN, DC12 and Lock In ice core drillings. We are grateful to drillers and field teams. We thank Michel Ramonet, Olivier Laurent, Luc Lienhardt and the entire team of the Integrated Carbon Observation System (ICOS) at LSCE for the time spent during the calibration of the OF-CEAS SARA spectrometer in September 2020. The TALos Dome Ice CorE (TALDICE) project, a joint European programme, is funded by national contributions from Italy, France, Germany, Switzerland and the United Kingdom. Primary logistical support was provided by PNRA at Talos Dome. This work is TALDICE publication no. 62.

Financial support. This work was supported by the following programs: the French ANR projects RPD-COCLICO (#10-RPDOC-002-01, X.F.), the EU grants FP7-IP #ENV-2010/265148 (project Pegasos, X.F.) and FP7 ERC #291062 (project Ice&Lasers, J.C.), the US NSF awards #0221515 (J.R.M.), #0909541 (J.R.M.), #1204176 (J.R.M.), #1406219 (J.R.M.), and #0968391 (E.B., Partnerships in International Research and Education, project PIRE). R. H. received funding from Issac Newton Trust Project LBZG/080. We thank the Australian Antarctic Science Program and the Australian Antarctic Division for support of drilling programs and atmospheric measurements (AAS Project 4621) and the Australian Bureau of Meteorology for air sampling at Mawson.

References

Acosta Navarro, J. C., Smolander, S., Struthers, H., Zorita, E., Ekman, A. M. L., Kaplan, J. O., Guenther, A., Arneth, A. and Riipinen, I.: Global emissions of terpenoid VOCs from terrestrial vegetation in the last millennium, J. Geophys. Res. Atmos., 119(11), 6867–6885, doi:10.1002/2013JD021238, 2014.

Allan, D. W.: Statistics of atomic frequency standards, Proc. IEEE, 54(2), 221–230, doi:10.1109/PROC.1966.4634, 1966.

Andela, N., Morton, D. C., Giglio, L., Chen, Y., van der Werf, G. R., Kasibhatla, P. S., DeFries, R. S., Collatz, G. J., Hantson, S., Kloster, S., Bachelet, D., Forrest, M., Lasslop, G., Li, F., Mangeon, S., Melton, J. R., Yue, C. and Randerson, J. T.: A human-driven decline in global burned area, Science, 356(6345), 1356–1362, doi:10.1126/science.aal4108, 2017.

Archibald, S., Lehmann, C. E. R., Belcher, C. M., Bond, W. J., Bradstock, R. A., Daniau, A. L., Dexter, K. G., Forrestel, E. J., Greve, M., He, T., Higgins, S. I., Hoffmann, W. A., Lamont, B. B., McGlinn, D. J., Moncrieff, G. R., Osborne, C. P., Pausas, J. G., Price, O., Ripley, B. S., Rogers, B. M., Schwilk, D. W., Simon, M. F., Turetsky, M. R., Van Der Werf, G. R., and Zanne, A.: Biological and geophysical feedbacks with fire in the Earth system. Environ. Res. Lett., 13, 033003, https://doi.org/10.1088/1748-9326/aa9ead, 2018.

Assonov, S. S., Brenninkmeijer, C. A. M., Jockel, P. J., Mulvaney, R., Bernard, S. and Chappellaz, J.: Evidence for a CO increase in the SH during the 20th century based on firn air samples from Berkner Island, Antarctica, Atmos. Chem. Phys., 7, 295–308, 2007.

https://doi.org/10.5194/cp-2023-9
Preprint. Discussion started: 21 April 2023

Bisiaux, M. M., Edwards, R., McConnell, J. R., Curran, M. A. J., Ommen, T. D. Van, Smith, A. M., Neumann, T. A., Pasteris, D. R., Penner, J. E. and Taylor, K.: Changes in black carbon deposition to Antarctica from two high-resolution ice core records , 1850 – 2000 AD, Atmos. Chem. Phys., 12, 4107–4115, doi:10.5194/acp-12-4107-2012, 2012.

Battle, M. O., Bender, M., Sowers, T., Tans, P. P., Butler, J. H., Elkins, J. W., Ellis, J. T., Conway, T., Zhang, N., Lang, P. and Clarke, A. D.: Atmospheric gas concentrations over the past century measured in air from firn at the South Pole, Nature, 383, 231–235, 1996.

Bock, M., Schmitt, J., Beck, J., Seth, B., Chappellaz, J. and Fischer, H.: Glacial/interglacial wetland, biomass burning, and geologic methane emissions constrained by dual stable isotopic CH_4 ice core records., Proc. Natl. Acad. Sci. U. S. A., 114(29), 2018

Bowman, D. M. J. S., Balch, J. K., Artaxo, P., Bond, W. J., Carlson, J. M., Cochrane, M. A., D'Antonio, C. M., DeFries, R. S., Doyle, J. C., Harrison, S. P., Johnston, F. H., Keeley, J. E., Krawchuk, M. A., Kull, C. A., Marston, J. B., Moritz, M. A., Prentice, I. C., Roos, C. I., Scott, A. C., Swetnam, T. W., van der Werf, G. R., and Pyne, S. J.: Fire in the Earth System, Science, 324, 481–484, https://doi.org/10.1126/science.1163886, 2009.

Butler, J. H., Montzka S. A., Battle M., Clarke A. D., Mondeel D. J., Lind J. A., Hall B. D., and Elkins J. W.: Collection and analysis of firn air from the South Pole, Abstract A51F-0145 presented at 2001 Fall Meeting, San Francisco (CA, USA), AGU, 2001.

Collins, W. J., Lamarque, J.-F., Schulz, M., Boucher, O., Eyring, V., Hegglin, M. I., Maycock, A., Myhre, G., Prather, M., Shindell, D. and Smith, S. J.: AerChemMIP: quantifying the effects of chemistry and aerosols in CMIP6, Geosci. Model Dev., 10(2), 585–607, doi:10.5194/gmd-10-585-2017, 2017.

Conte, L., Szopa, S., Séférian, R. and Bopp, L.: The oceanic cycle of carbon monoxide and its emissions to the atmosphere, Biogeosciences, 16(4), 881–902, doi:10.5194/bg-16-881-2019, 2019.

Crutzen, P. J.: A discussion of the chemistry of some minor constituents in the stratosphere and troposphere, Pure Appl. Geophys., 106–108(1), 1385–1399, doi:10.1007/BF00881092, 1973.

Dlugokencky, E. J., Nisbet, E. G., Fisher, R. and Lowry, D.: Global atmospheric methane: budget, changes and dangers, Philos. Trans. A. Math. Phys. Eng. Sci., 369(1943), 2058–72, doi:10.1098/rsta.2010.0341, 2011.

Duncan, B., Logan, J. A., Bey, I., Megretskaia, I. A., Yantosca, R. M., Novelli, P. C., Jones, N. B. and Rinsland, C. P.: Global budget of CO, 1988-1997: Source estimates and validation with a global model, J. Geophys. Res., 112(D22), doi:10.1029/2007jd008459, 2007.

Etheridge, D. M., Steele, L. P., Langenfelds, R. L., Francey, R. J., Barnola, J. M. and Morgan, V. I.: Natural and anthropogenic changes in atmospheric CO_2 over the last 1000 years from air in Antarctic ice and firn, J. Geophys. Res., 101(D2), 4115–4128, 1996.

Fabre, A., Barnola, J. M., Arnaud, L. and Chappellaz, J.: Determination of gas diffusivity in polar firn: comparison between experimental measurements and inverse modeling, Geophys. Res. Lett., 27(4), 557–560, 2000.

Faïn, X., Chappellaz, J., Rhodes, R. H., Stowasser, C., Blunier, T., McConnell, J. R., Brook, E. J., Preunkert, S., Legrand, M., Debois, T. and Romanini, D.: High resolution measurements of carbon monoxide along a late Holocene Greenland ice core: evidence for in situ production, Clim. Past, 10(3), 987–1000, doi:10.5194/cp-10-987-2014, 2014.

Faïn, X., Rhodes, R. H., Place, P., Petrenko, V. V., Fourteau, K., Chellman, N., Crosier, E., McConnell, J. R., Brook, E. J., Blunier, T., Legrand, M. and Chappellaz, J.: Northern Hemisphere atmospheric history of carbon monoxide since preindustrial times reconstructed from multiple Greenland ice cores, Clim. Past, 18(3), 631–647, doi:10.5194/cp-18-631-2022, 2022.

Ferretti, D. F., Miller, J. B., White, J. W. C., Etheridge, D. M., Lassey, K. R., Lowe, D. C., Meure, C. M. M., Dreier, M. F., Trudinger, C. M., van Ommen, T. D. and Langenfelds, R. L.: Unexpected changes to the global methane budget over the past 2000 years, Science (80-.)., 309(5741), 1714–1717, doi:10.1126/science.1115193, 2005.

Fourteau, K., Martinerie, P., Faïn, X., Schaller, C. F., Tuckwell, R. J., Löwe, H., Arnaud, L., Magand, O., Thomas, E. R., Freitag, J., Mulvaney, R., Schneebeli, M. and Lipenkov, V. Y.: Multi-tracer study of gas trapping in an East Antarctic ice core, Cryosph., 13(12), 3383–3403, doi:10.5194/tc-13-3383-2019, 2019.

Fourteau, K., Martinerie, P., Faïn, X., Ekaykin, A. A., Chappellaz, J. and Lipenkov, V.: Estimation of gas record alteration in very low-accumulation ice cores, Clim. Past, 16(2), 503–522, doi:10.5194/cp-16-503-2020, 2020.

Frezzotti, M., Urbini, S., Proposito, M., Scarchilli, C. and Gandolfi, S.: Spatial and temporal variability of surface mass balance near Talos Dome, East Antarctica, J. Geophys. Res. Earth Surf., doi:10.1029/2006JF000638, 2007.

Gautier, E., Savarino, J., Erbland, J., Lanciki, A. and Possenti, P.: Variability of sulfate signal in ice core records based on five replicate cores, Clim. Past, 12(1), 103–113, doi:10.5194/cp-12-103-2016, 2016.

Guenther, A., Hewitt, C. N., Erickson, D., Fall, R., Geron, C., Graedel, T., Harley, P., Klinger, L., Lerdau, M., Mckay, W. A., Pierce, T., Scholes, B., Steinbrecher, R., Tallamraju, R., Taylor, J. and Zimmerman, P.: A global model of natural volatile organic compound emissions, J. Geophys. Res., 100(D5), 8873, doi:10.1029/94JD02950, 1995.

Guenther, A. B., Jiang, X., Heald, C. L., Sakulyanontvittaya, T., Duhl, T., Emmons, L. K. and Wang, X.: The Model of Emissions of Gases and Aerosols from Nature version 2.1 (MEGAN2.1): an extended and updated framework for modeling biogenic emissions, Geosci. Model Dev., 5(6), 1471–1492, doi:10.5194/gmd-5-1471-2012, 2012.

Goldewijk, K. K., Beusen, A., Doelman, J. and Stehfest, E.: Anthropogenic land use estimates for the Holocene – HYDE 3.2, Earth Syst. Sci. Data, 9(2), 927–953, doi:10.5194/essd-9-927-2017, 2017.

Haan, D., Martinerie, P. and Raynaud, D.: Ice core data of atmospheric carbon monoxide over Antarctica and Greenland during the last 200 years, Geophys. Res. Lett., 23(17), 2235–2238, 1996.

Haan, D. and Raynaud, D.: Ice core record of CO variations during the last two millennia: atmospheric implications and chemical interactions within the Greenland ice, Tellus Ser. B-Chemical Phys. Meteorol., 50(3), 253–262, 1998.

Hamilton, D. S., Hantson, S., Scott, C. E., Kaplan, J. O., Pringle, K. J., Nieradzik, L. P., Rap, A., Folberth, G. A., Spracklen, D. V. and Carslaw, K. S.: Reassessment of pre-industrial fire emissions strongly affects anthropogenic aerosol forcing, Nat. Commun., 9(1), 3182, doi:10.1038/s41467-018-05592-9, 2018.

Hantson, S., Knorr, W., Schurgers, G., Pugh, T. A. M. and Arneth, A.: Global isoprene and monoterpene emissions under changing climate, vegetation, CO_2 and land use, Atmos. Environ., 155, 35–45, doi:10.1016/j.atmosenv.2017.02.010, 2017.

Helmig, D., Petrenko, V. V., Martinerie, P., Witrant, E., Röckmann, T., Zuiderweg, A., Holzinger, R., Hueber, J., Thompson, C., White, J. W. C., Sturges, W. T., Baker, A., Blunier, T., Etheridge, D. M., Rubino, M. and Tans, P.: Reconstruction of Northern Hemisphere 1950–2010 atmospheric non-methane hydrocarbons, Atmos. Chem. Phys., 14(3), 1463–1483, doi:10.5194/acp-14-1463-2014, 2014.

Knorr, W., Kaminski, T., Arneth, A. and Weber, U.: Impact of human population density on fire frequency at the global scale, Biogeosciences, 11(4), 1085–1102, doi:10.5194/bg-11-1085-2014, 2014.

Laube, J. C., Mohd Hanif, N., Martinerie, P., Gallacher, E., Fraser, P. J., Langenfelds, R., Brenninkmeijer, C. A. M., Schwander, J., Witrant, E., Wang, J.-L., Ou-Yang, C.-F., Gooch, L. J., Reeves, C. E., Sturges, W. T. and Oram, D. E.: Tropospheric observations of CFC-114 and CFC-114a with a focus on long-term trends and emissions, Atmos. Chem. Phys., 16(23), 15347–15358, doi:10.5194/acp-16-15347-2016, 2016.

Langenfelds, R. L., Guerette E-A., Steele L. P., Krummel P. B., Spencer D. A., Loh Z. M., Gregory R. L., Thornton D. P., Howden R. T. and Fraser P. J.: Atmospheric methane, carbon dioxide, carbon monoxide, hydrogen and nitrous oxide from Cape Grim flask samples analysed by gas chromatography, in Baseline Atmospheric Program (Australia), 2014-16, R. Langenfelds, N. Derek and S. L. Cleland (eds.), Bureau of Meteorology and CSIRO Environment, Melbourne, Australia, 2023.

Loh, Z., Langenfelds, R. and Krummel, P.: Atmospheric CO at Casey by Commonwealth Scientific and Industrial Research Organisation, dataset published as CO_CYA_surface-flask_CSIRO_data1 at WDCGG, ver.2021-04-08-1004, https://doi.org/10.50849/WDCGG_0016-7004-3001-01-02-9999, 2021a.

Loh, Z., Langenfelds, R. and Krummel, P.: Atmospheric CO at South Pole by Commonwealth Scientific and Industrial Research Organisation, dataset published as CO_SPO_surface-flask_CSIRO_data1 at WDCGG, ver.2021-04-08-1004, https://doi.org/10.50849/WDCGG_0016-7011-3001-01-02-9999, 2021b.

Loh, Z., Langenfelds, R. and Krummel, P.: Atmospheric CO at Mawson by Commonwealth Scientific and Industrial Research Organisation, dataset published as CO_MAA_surface-flask_CSIRO_data1 at WDCGG, ver.2021-04-08-1004, https://doi.org/10.50849/WDCGG_0016-7005-3001-01-02-9999, 2021c.

Legrand, M., McConnell, J. R., Fischer, H., Wolff, E. W., Preunkert, S., Arienzo, M. M., Chellman, N., Leuenberger, D., Maselli, O. J., Place, P., Sigl, M., Schupbach, S. and Flannigan, M.: Boreal fire records in Northern Hemisphere ice cores: A review, Clim. Past, 12(10), 2033–2059, doi:10.5194/cp-12-2033-2016, 2016.

Lelieveld, J., Gromov, S., Pozzer, A. and Taraborrelli, D.: Global tropospheric hydroxyl distribution, budget and reactivity, Atmos. Chem. Phys., 16(19), 12477–12493, doi:10.5194/acp-16-12477-2016, 2016.

Liu, P., Kaplan, J. O., Mickley, L. J., Li, Y., Chellman, N. J., Arienzo, M. M., Kodros, J. K., Pierce, J. R., Sigl, M., Freitag, J., Mulvaney, R., Curran, M. A. J. and Mcconnell, J. R.: Improved estimates of preindustrial biomass burning reduce the magnitude of aerosol climate forcing in the Southern Hemisphere, Science Advance, 2021.

Lukas, M. A.: Strong robust generalized cross-validation for choosing the regularization parameter, Inverse Probl., 24(3), 034006, doi:10.1088/0266-5611/24/3/034006, 2008.

Marlon, J. R., Bartlein, P. J., Carcaillet, C., Gavin, D. G., Harrison, S. P., Higuera, P. E., Joos, F., Power, M. J. and Prentice, I. C.: Climate and human influences on global biomass burning over the past two millennia, Nat. Geosci., 1(10), 697–702, doi:10.1038/ngeo313, 2008.

Marlon, J. R., Bartlein, P. J., Daniau, A.-L., Harrison, S. P., Maezumi, S. Y., Power, M. J., Tinner, W. and Vannière, B.: Global biomass burning : a synthesis and review of Holocene paleo fire records and their controls, Quat. Sci. Rev., 65, 5–25, 2013

Marlon, J. R., Kelly, R., Daniau, A.-L., Vannière, B., Power, M. J., Bartlein, P., Higuera, P., Blarquez, O., Brewer, S., Brücher, T., Feurdean, A., Romera, G. G., Iglesias, V., Maezumi, S. Y., Magi, B., Courtney Mustaphi, C. J. and Zhihai, T.: Reconstructions of biomass burning from sediment-charcoal records to improve data–model comparisons, Biogeosciences, 2016.

McConnell, J. R., Chellman, N. J., Mulvaney, R., Eckhardt, S., Stohl, A., Plunkett, G., Kipfstuhl, S., Freitag, J., Isaksson, E., Gleason, K. E., Brugger, S. O., McWethy, D. B., Abram, N. J., Liu, P. and Aristarain, A. J.: Hemispheric black carbon increase after the 13th-century Māori arrival in New Zealand, Nature, 598(7879), 82–85, doi:10.1038/s41586-021-03858-9, 2021.

Mischler, J. A., Sowers, T. A., Alley, R. B., Battle, M., McConnell, J. R., Mitchell, L. E., Popp, T., Sofen, E. and Spencer, M. K.: Carbon and hydrogen isotopic composition of methane over the last 1000 years, Global Biogeochem. Cycles, 23(4), 2009.

Mulvaney, R., Oerter, H., Peel, D. A., Graf, W., Arrowsmith, C., Pasteur, E. C., Knight, B., Littot, G. C. and Miners, W. D.: 1000 year ice-core records from Berkner Island, Antarctica, Ann. Glaciol., 35, 45–51, doi:10.3189/172756402781817176, 2002.

Murray, L. T., Mickley, L. J., Kaplan, J. O., Sofen, E. D., Pfeiffer, M. and Alexander, B.: Factors controlling variability in the oxidative capacity of the troposphere since the Last Glacial Maximum, Atmos. Chem. Phys., 14(7), 3589–3622, doi:10.5194/acp-14-3589-2014, 2014.

Nicewonger, M. R., Aydin, M., Prather, M. J. and Saltzman, E. S.: Large changes in biomass burning over the last millennium inferred from paleoatmospheric ethane in polar ice cores, Proc. Natl. Acad. Sci., 201807172, doi:10.1073/pnas.1807172115, 2018.

Nicewonger, M. R., Aydin, M., Prather, M. J. and Saltzman, E. S.: Reconstruction of paleofire emissions over the past millennium from measurements of ice core acetylene, Geophys. Res. Lett., 47(3), doi:10.1029/2019GL085101, 2020a.

Nicewonger, M. R., Aydin, M., Prather, M. J. and Saltzman, E. S.: Extracting a history of global fire emissions for the past millennium from ice core records of acetylene, Ethane, and Methane, J. Geophys. Res. Atmos., 125(20), doi:10.1029/2020JD032932, 2020b.

Pan, X., Ichoku, C., Chin, M., Bian, H., Darmenov, A., Colarco, P., Ellison, L., Kucsera, T., da Silva, A., Wang, J., Oda, T. and Cui, G.: Six global biomass burning emission datasets: intercomparison and application in one global aerosol model, Atmos. Chem. Phys., 20(2), 969–994, doi:10.5194/acp-20-969-2020, 2020.

Pongratz, J., Reick, C., Raddatz, T. and Claussen, M.: A reconstruction of global agricultural areas and land cover for the last millennium, Global Biogeochem. Cycles, 22(3), GB3018, doi:10.1029/2007GB003153, 2008.

Power, M. J., Marlon, J. R., Ortiz, N., Bartlein, P. J., Harrison, S. P., Mayle, F. E., Ballouche, a., Bradshaw, R. H. W., Carcaillet, C., Cordova, C., Mooney, S., Moreno, P. I., Prentice, I. C., Thonicke, K., Tinner, W., Whitlock, C., Zhang, Y., Zhao, Y., Ali, a. a., Anderson, R. S., Beer, R., Behling, H., Briles, C., Brown, K. J., Brunelle, a., Bush, M., Camill, P., Chu, G. Q., Clark, J., Colombaroli, D., Connor, S., Daniau, A.-L., Daniels, M., Dodson, J., Doughty, E., Edwards, M. E., Finsinger, W., Foster, D., Frechette, J., Gaillard, M.-J. J., Gavin, D. G., Gobet, E., Haberle, S., Hallett, D. J., Higuera, P., Hope, G., Horn, S., Inoue, J., Kaltenrieder, P., Kennedy, L., Kong, Z. C., Larsen, C., Long, C. J., Lynch, J., Lynch, E. a., McGlone, M., Meeks, S., Mensing, S., Meyer, G., Minckley, T., Mohr, J., Nelson, D. M., New, J., Newnham, R., Noti, R., Oswald, W., Pierce, J., Richard, P. J. H., Rowe, C., Sanchez Goñi, M. F., Shuman, B. N., Takahara, H., Toney, J., Turney, C., Urrego-Sanchez, D. H., Umbanhowar, C., Vandergoes, M., Vannière, B., Vescovi, E., Walsh, M., Wang, X., Williams, N., Wilmshurst, J., Zhang, J. H. and Goni, M. F. S.: Changes in fire regimes since the Last Glacial Maximum: an assessment based on a global synthesis and analysis of charcoal data, Clim. Dyn., 30(7–8), 887–907, doi:10.1007/s00382-007-0334-x, 2008.

Power, M. J., Mayle, F., Bartlein, P., Marlon, J. R., Anderson, R., Behling, H., Brown, K., Carcaillet, C., Colombaroli, D., Gavin, D., Hallett, D., Horn, S., Kennedy, L., Lane, C., Long, C., Moreno, P., Paitre, C., Robinson, G. S., Taylor, Z. and Walsh, M.: Climatic control of the biomass-burning decline in the Americas after AD 1500, The Holocene, 23(1), 3–13, doi:10.1177/0959683612450196, 2012.

Rommelaere, V., Arnaud, L. and Barnola, J. M.: Reconstructing recent atmospheric trace gas concentrations from polar firn and bubbly ice data by inverse methods, J. Geophys. Res., 102, 30 069-30 083, 1997.

Rowlinson, M. J., Rap, A., Hamilton, D. S., Pope, R. J., Hantson, S., Arnold, S. R., Kaplan, J. O., Arneth, A., Chipperfield, M. P., Forster, P. M. and Nieradzik, L.: Tropospheric ozone radiative forcing uncertainty due to pre-industrial fire and biogenic emissions, Atmos. Chem. Phys., 20(18), 10937–10951, doi:10.5194/acp-20-10937-2020, 2020.

Rubino, M., D'Onofrio, A., Seki, O. and Bendle, J. A.: Ice-core records of biomass burning, Anthr. Rev., 3(2), 140–162, doi:10.1177/2053019615605117, 2016a.

Rubino, M., Etheridge, D. M., Trudinger, C. M., Allison, C. E., Rayner, P. J., Enting, I., Mulvaney, R., Steele, L. P., Langenfelds, R. L., Sturges, W. T., Curran, M. A. J. and Smith, A. M.: Low atmospheric CO_2 levels during the Little Ice Age due to cooling induced terrestrial uptake, Nat. Geosci., 9(9), 691–694, doi:10.1038/ngeo2769, 2016b.

Rubino, Mauro; Etheridge, David; Thornton, David; Howden, Russell; Allison, Colin; Francey, Roger; et al. Revised records of atmospheric trace gases CO_2, CH_4, N_2O and ^{13}C-CO_2 over the last 2000 years from Law Dome, Antarctica. Earth System Science Data.: 11:473-492,doi.org/10.5194/essd-11-473-2019, 2019.

Sapart, C. J., Monteil, G., Prokopiou, M., van de Wal, R. S. W., Kaplan, J. O., Sperlich, P., Krumhardt, K. M., van der Veen, C., Houweling, S., Krol, M. C., Blunier, T., Sowers, T. A., Martinerie, P., Witrant, E., Dahl-Jensen, D. and Rockmann, T.: Natural and anthropogenic variations in methane sources during the past two millennia, Nature, 490(7418), 85–88, doi:Doi 10.1038/Nature11461, 2012.

https://doi.org/10.5194/cp-2023-9
Preprint. Discussion started: 21 April 2023

Servettaz, A., Orsi, A. J., Curran, M. A. J., Moy, A. D., Landais, A., Agosta, C., Winton, V. H. L., Touzeau, A., McConnell, J. R., Werner, M. and Baroni, M.: Snowfall and Water Stable Isotope Variability in East Antarctica Controlled by Warm Synoptic Events, J. Geophys. Res. Atmos., 125(17), e2020JD032863, doi:10.1029/2020JD032863, 2020.

Servettaz, A. P. M., Orsi, A. J., Curran, M. A. J., Moy, A. D., Landais, A., McConnell, J. R., Popp, T. J., Le Meur, E., Faïn, X. and Chappelaz, J.: A 2000-year temperature reconstruction on the East Antarctic plateau, from argon-nitrogen and water stable isotopes in the Aurora Basin North ice core, Clim. Past Discuss., 2022, 1–58, doi:10.5194/cp-2022-91, 2022.

Stenni, B., Proposito, M., Gragnani, R., Flora, O., Jouzel, J., Falourd, S. and Frezzotti, M.: Eight centuries of volcanic signal and climate change at Talos Dome (East Antarctica), J. Geophys. Res. Atmos., 107(D9), ACL 3-1-ACL 3-13, doi:10.1029/2000JD000317, 2002.

Sturrock, G. A.; Etheridge, D. M.; Trudinger, C. M.; Fraser, P. J.; Smith, A. M.: Atmospheric histories of halocarbons from analysis of Antarctic firn air: Major Montreal Protocol species. Journal of geophysical research - Atmospheres. 107(D24):4765, doi:10.1029/2002JD002548, 2002.

Schwander, J., Barnola, J. M., Andrie, C., Leuenberger, M., Ludin, A., Raynaud, D. and Stauffer, B.: The age of the air in the firn and the ice at Summit, Greenland, J. Geophys. Res., 98, 2831–2838, 1993.

Stevenson, D. S., Zhao, A., Naik, V., O'Connor, F. M., Tilmes, S., Zeng, G., Murray, L. T., Collins, W. J., Griffiths, P. T., Shim, S., Horowitz, L. W., Sentman, L. T. and Emmons, L.: Trends in global tropospheric hydroxyl radical and methane lifetime since 1850 from AerChemMIP, Atmos. Chem. Phys., 20(21), 12905–12920, doi:10.5194/acp-20-12905-2020, 2020.

Szopa, S., V. Naik, B. Adhikary, P. Artaxo, T. Berntsen, W.D. Collins, S. Fuzzi, L. Gallardo, A. Kiendler-Scharr, Z. Klimont, H. Liao, N. Unger, and P. Zanis, 2021: Short-Lived Climate Forcers. In Climate Change 2021: The Physical Science Basis. Contribution of Working Group I to the Sixth Assessment Report of the Intergovernmental Panel on Climate Change [Masson-Delmotte, V., P. Zhai, A. Pirani, S.L. Connors, C. Péan, S. Berger, N. Caud, Y. Chen, L. Goldfarb, M.I. Gomis, M. Huang, K. Leitzell, E. Lonnoy, J.B.R. Matthews, T.K. Maycock, T. Waterfield, O. Yelekçi, R. Yu, and B. Zhou (eds.)]. Cambridge University Press, Cambridge, United Kingdom and New York, NY, USA, pp. 817–922, doi:10.1017/9781009157896.008.

Tarr, M. A., Miller, W. L. and Zepp, R. G.: Direct carbon monoxide photoproduction from plant matter, J. Geophys. Res., 100(D6), 11403, doi:10.1029/94JD03324, 1995.

Thoning, K. W., Tans, P. P., and Komhyr, W. D., Atmospheric carbon dioxide at Mauna Loa Observatory: 2. Analysis of the NOAA GMCC data, 1974–1985, J. Geophys. Res., 94(D6), 8549– 8565, doi:10.1029/JD094iD06p08549, 1989.

Trudinger, C. M., Enting, I. G., Etheridge, D. M., Francey, R. J., Levchenko, V. A., Steele, L. P., Raynaud, D., and Arnaud, L.: Modeling air movement and bubble trapping in firn, J. Geophys. Res., 102, 6747–6763, 1997.

Trudinger, C. M., Etheridge, D. M., Rayner, P. J., Enting, I. G., Sturrock, G. A., and Langenfelds, R. L.: Reconstructing atmospheric histories from measurements of air composition in firn, J. Geophys. Res., 107, 4780, doi:10.1029/2002JD002545, 2002.

https://doi.org/10.5194/cp-2023-9
Preprint. Discussion started: 21 April 2023

Climate of the Past Discussions

Trudinger, C. M., Enting, I. G., Rayner, P. J., Etheridge, D. M., Buizert, C., Rubino, M., Krummel, P. B., and Blunier, T.: How well do different tracers constrain the firn diffusivity profile?, Atmos. Chem. Phys., 13, 1485–1510, doi:10.5194/acp-13-1485-2013, 2013.

Trudinger, C. M., Fraser, P. J., Etheridge, D. M., Sturges, W. T., Vollmer, M. K., Rigby, M., Martinerie, P., Mühle, J., Worton, D. R., Krummel, P. B., Steele, L. P., Miller, B. R., Laube, J., Mani, F. S., Rayner, P. J., Harth, C. M., Witrant, E., Blunier, T., Schwander, J., O'Doherty, S. and Battle, M.: Atmospheric abundance and global emissions of perfluorocarbons CF_4, C_2F_6 and C_3F_8 since 1800 inferred from ice core, firn, air archive and in situ measurements, Atmos. Chem. Phys., 16(18), 11733–11754, doi:10.5194/acp-16-11733-2016, 2016.

van der Werf, G. R., Randerson, J. T., Giglio, L., Collatz, G. J., Mu, M., Kasibhatla, P. S., Morton, D. C., DeFries, R. S., Jin, Y. and van Leeuwen, T. T.: Global fire emissions and the contribution of deforestation, savanna, forest, agricultural, and peat fires (1997–2009), Atmos. Chem. Phys., 10(23), 11707–11735, doi:10.5194/acp-10-11707-2010, 2010.

van der Werf, G. R., Peters, W., van Leeuwen, T. T. and Giglio, L.: What could have caused pre-industrial biomass burning emissions to exceed current rates?, Clim. Past, 9(1), 289–306, doi:10.5194/cp-9-289-2013, 2013.

van der Werf, G. R., Randerson, J. T., Giglio, L., van Leeuwen, T. T., Chen, Y., Rogers, B. M., Mu, M., van Marle, M., Morton, D. C., Collatz, G. J., Yokelson, R. J. and Kasibhatla, P. S.: Global fire emissions estimates during 1997–2016, Earth Syst. Sci. Data, 9(2), 697–720, doi:10.5194/essd-9-697-2017, 2017.

van Marle, M., Kloster, S., Magi, B. I., Marlon, J. R., Daniau, A.-L., Field, R. D., Arneth, A., Forrest, M., Hantson, S., Kehrwald, N. M., Knorr, W., Lasslop, G., Li, F., Mangeon, S., Yue, C., Kaiser, J. W. and van der Werf, G. R.: Historic global biomass burning emissions for CMIP6 (BB4CMIP) based on merging satellite observations with proxies and fire models (1750–2015), Geosci. Model Dev., 10(9), 3329–3357, doi:10.5194/gmd-10-3329-2017, 2017.

Vannière, B., Blarquez, O., Rius, D., Doyen, E., Brücher, T., Colombaroli, D., Connor, S., Feurdean, A., Hickler, T., Kaltenrieder, P., Lemmen, C., Leys, B., Massa, C. and Olofsson, J.: 7000-year human legacy of elevation-dependent European fire regimes, Quat. Sci. Rev., 132, 206–212, doi:10.1016/J.QUASCIREV.2015.11.012, 2016.

Wang, Z., Chappellaz, J., Park, J. Y. and Mak, J.: Large variations in Southern Hemisphere biomass burning during the last 650 years, Science, 330, 1663–166, doi:10.1126/science.1197257, 2010.

Werle, P., Mücke, R. and Slemr, F.: The Limits of Signal Averaging in Atmospheric Trace-Gas Monitoring by Tunable Diode-Laser Absorption Spectroscopy (TDLAS), Appl. Phys. B-Lasers Opt., 139, 131–139, 1993.

Witrant, E., Martinerie, P., Hogan, C., Laube, J. C., Kawamura, K., Capron, E. and Montzka, S. A., E. J. Dlugokencky,D. Etheridge, T. Blunier, and W. T. Sturges: A new multi-gas constrained model of trace gas non-homogeneous transport in firn : evaluation and behaviour at eleven polar sites, Atmos. Chem. Phys., (12), 11465–11483, doi:10.5194/acp-12-11465-2012, 2012.

Worton, D. R., Sturges, W. T., Gohar, L. K., Shine, K. P., Martinerie, P., Oram, D. E., Humphrey, S. P., Begley, P., Gunn, L., Barnola, J. M., Schwander, J. and Mulvaney, R.: Atmospheric Trends and Radiative Forcings of CF_4 and C_2F_6 Inferred from Firn Air, Environ. Sci. Technol., 41(7), 2184–2189, doi:10.1021/es061710t, 2007.

https://doi.org/10.5194/cp-2023-9
Preprint. Discussion started: 21 April 2023

Climate of the Past Discussions Open Access

Yeung, L. Y., Murray, L. T., Martinerie, P., Witrant, E., Hu, H., Banerjee, A., Orsi, A. and Chappellaz, J.: Isotopic constraint
1050 on the twentieth-century increase in tropospheric ozone, Nature, 570(7760), 224–227, doi:10.1038/s41586-019-1277-1, 2019.